

SANDIA REPORT

SAND99-0714

Unlimited Release

Printed April 1999

Kovar Micro Heat Pipe Substrates for Microelectronic Cooling

**David A. Benson, Steven N. Burchett, Stanley H. Kravitz,
Chris P. Tigges, Carrie Schmidt and Charles V. Robino**

Prepared by

Sandia National Laboratories

Albuquerque, New Mexico 87185 and Livermore, California 94550

for the United States Department of Energy

under Contract DE-AC04-94AL85000

Approved for public release; further dissemination unlimited.

Issued by Sandia National Laboratories, operated for the United States Department of Energy by Sandia Corporation.

NOTICE: This report was prepared as an account of work sponsored by an agency of the United States Government. Neither the United States Government nor any agency thereof, nor any of their employees, nor any of their contractors, subcontractors, or their employees, makes any warranty, express or implied, or assumes any legal liability or responsibility for the accuracy, completeness, or usefulness of any information, apparatus, product, or process disclosed, or represents that its use would not infringe privately owned rights. Reference herein to any specific commercial product, process, or service by trade name, trademark, manufacturer, or otherwise, does not necessarily constitute or imply its endorsement, recommendation, or favoring by the United States Government, any agency thereof, or any of their contractors or subcontractors. The views and opinions expressed herein do not necessarily state or reflect those of the United States Government, any agency thereof, or any of their contractors.

Printed in the United States of America. This report has been reproduced directly from the best available copy.

Available to DOE and DOE contractors from
Office of Scientific and Technical Information
P.O. Box 62
Oak Ridge, TN 37831

Prices available from (615) 576-8401, FTS 626-8401

Available to the public from
National Technical Information Service
U.S. Department of Commerce
5285 Port Royal Rd
Springfield, VA 22161

NTIS price codes
Printed copy: A11
Microfiche copy: A01



SAND99-0714
Unlimited Release
Printed April 1999

Kovar Micro Heat Pipe Substrates for Microelectronic Cooling

David A. Benson
Advanced Electronic Packaging Department

Steven N. Burchett
Engineering and Manufacturing Mechanics Department

Stanley H. Kravitz, Chris P. Tigges and Carrie Schmidt
Adv. Semiconductor Technology Department

Charles V. Robino
Materials Joining Department

Sandia National Laboratories
P.O. Box 5800
Albuquerque, NM 87185-1082

Abstract

We describe the development of a new technology for cooling microelectronics. This report documents the design, fabrication, and prototype testing of micro scale heat pipes embedded in a flat plate substrate or heat spreader. A thermal model tuned to the test results enables us to describe heat transfer in the prototype, as well as evaluate the use of this technology in other applications. The substrate walls are Kovar alloy, which has a coefficient of thermal expansion close to that of microelectronic die. The prototype designs integrating micro heat pipes with Kovar enhance thermal conductivity by more than a factor of two over that of Kovar alone, thus improving the cooling of microelectronic die.

Contents

Introduction.....	1
Background: Traditional Methods for Cooling Microelectronics	2
The Micro Heat Pipe Substrate: A New Approach to Cooling.....	3
Design of Wick Patterns	4
Wick Spacing.....	4
Double Layer Wick Design	6
Photo Lithography and Plating Processes.....	10
Heat Pipe Materials and Assembly.....	14
Background.....	14
Fabrication Procedures	16
Alternate Fill Tube Configurations.....	22
Coolant fill process	26
Material Compatibility between Wall and Coolant	27
Mechanical Design and Wall Deformation	29
Analytic Assessment.....	30
Finite Element Model	31
Summary of the Wall Analysis.....	32
Thermal Testing.....	32
Test Die Measurements	32
IR measurements.....	33
Initial Test Results	34
Radial Profile Wick Test.....	35
Discussion.....	40
References.....	41
Appendix A: Parametric Database for the Radial Wick Designs	42
Appendix B: Wick Lithography Processes.....	44

Figures

Figure 1.	(left) Basic design of the heat pipe substrate: two plates with wick features on their inner surface are separated by spacers and sealed along the edges. (right) Enlargement of heat pipe wick features micromachined on wall surfaces.3
Figure 2.	Photoetched patterns used for the silicon substrate testing work. Dimensions are in microns. The features tested were 55 microns tall.5
Figure 3.	(left) Wick 1 layer (upper layer) resulting from scaling parameters 32x actual used values. This wick is intended for the thick flow regions of the heat pipe. (right) One octant of the wick 2 layer (lower layer) again at 32x normal scaling. Having finer features than wick 1, wick 2 is expected to enhance the flow where the fluid layer is thin and approaching the dry out stage.8
Figure 4.	(top) Wick 1 layer detail. (bottom) Similar detail including both wick layers. Both details are near a radial zone boundary. Compare with SEM details in Figure 5.9
Figure 5.	(left) SEM detail of center of heat pipe wick. (right) SEM detail near radial zone boundary clearly showing the two wick layers. The top wick layer has been overplated, providing additional height and corners. Compare SEM details with the mask design in Figure 4.10
Figure 6.	Diagram of the fountain plating system used for the nickel wick deposition... 13
Figure 7.	Initial frame design with integral supports. Dimensions are nominal.16
Figure 8.	Frame design used in latter heat pipes. Dimensions are nominal.17
Figure 9.	Schematic diagram of heat pipe assembly18
Figure 10.	Cross section of first internal spacer resistance weld.19
Figure 11.	Cross section of closure weld at the edge of the heat pipe substrate. Note that the weld melt zone spans the entire thickness of the substrate.20
Figure 12.	Cross section of second internal support resistance weld.21
Figure 13.	Schematic diagram of fill tube attachment to the heat pipe wall.22
Figure 14.	Mock-up of heat pipe used for fill tube attachment trials.23
Figure 15.	Diagram of direct solder seal joint.24
Figure 16.	Macro photograph of percussive arc weld tube attachment.25
Figure 17.	Cross sections of percussive arc weld: unetched (left), etched (right).26
Figure 18.	Finite element mesh for baseline structural computations.31
Figure 19.	Computed displacement contours for 0, 4, and 8 internal supports for substrate without die and with silicon die. The maximum displacement on the scale is 0.005 inches.31

Figure 20.	(left) Infrared imaging system and heat pipe mounting fixtures. (right) Detailed view of test fixture seen at the left on the thermal stage below the lens.	33
Figure 21.	Comparison of a Kovar heat pipe cooled surface (left) to the same geometry of surface without heat pipes (right).	35
Figure 22.	Photo of heated wall wick surface CD5/CD6 prototype at three positions ranging from the center (left) to the outer edge (right). The higher magnification photo at the far right shows the taller overplated cap layer near the edge.	36
Figure 23.	Front and back temperature maps for 2, 5 and 10 watts power input for the heated side (left) and the back side (right). The base temperature was 35°C for these tests on the CD5CD6 prototype.	37
Figure 24.	Plots of temperature profiles across CD5CD6 prototype heat pipe for the cases shown in Figure 23.	38
Figure 25.	Simulation of a one-eighth section of the CD5CD6 heat pipe geometry, including a die mounted at the center dissipating 5 watts and the edge constrained to a fixed temperature. The colors on the mesh at the left indicate the type of material; the mesh at the right shows a color-coded temperature map of the die and substrate surfaces.	39
Figure 26.	Comparison of temperature profiles from the model and from test results. The model is based on a constant interface heat transfer coefficient.....	39

Tables

Table 1.	Permeability and pumping capacity measured for the four patterns in Fig. 2. ..5
Table 2.	ASTM Chemical Requirements for Kovar Alloy.14
Table 3.	Resistance weld parameters for UNITEK 250DP welder.18
Table 4.	Weld parameters for Lumonics JK 704 Nd:YAG laser welder. These welds attached the front and back sides of the heat pipe substrate to make the hermetically sealed assembly.19
Table 5:	Displacements computed analytically for several substrate thicknesses.30
Table 6:	Computed support spacing to maintain displacement below 10% of the substrate thickness.30
Table 7:	Mechanical properties for the materials in the finite element analysis.....32

Acknowledgments

The authors wish to thank the staff of the microelectronics packaging and test labs for their assistance, J. Mulhall for his help in testing, S. Smith for her scanning electron microscopy, and T. Castillo for help in heat pipe filling. We also wish to thank the staff of the CSRL for assistance in the processing effort including electrodeposition of the heat pipe wicks.

Introduction

The fundamental need to improve cooling efficiency spans much of developing micro electronics technology. There is constant pressure on military electronics system designers to reduce system volume while increasing electronics complexity and power density. Compound semiconductor phased array radar modules are trending to higher power, smaller module size, and larger arrays. Additional needs for cooling opto electronics, laser diodes, high speed processors and communication equipment are increasingly demanding. Currently these systems use bulk conductive substrates to spread heat from hot components and to channel thermal energy to heat sinks. When applications involve higher heat fluxes, a pumped coolant approach is generally used.¹

Despite the migration from high power bipolar to low power CMOS logic, the lowering of device operating voltages, and the use of sleep mode in circuit design, the power density of microelectronics systems continues to increase: higher frequency clocks have made CMOS as power hungry as bipolar; low voltage has led to high current, high loss power conversion and transmission; and micro sensors and their heat-producing analog circuitry are proliferating.

Designers need a thermal management tool kit with many options to solve the many heat problems constraining advances in microelectronics technology today. The micro heat pipe substrate is a new tool that offers high cooling efficiency to solve such problems. This report describes the design, fabrication, and testing of thin, flat plate substrates containing micro scale heat pipes. By embedding passive micro heat pipes within the flat substrate, we can achieve high effective thermal conductivity for the spreading of heat across the area of the substrate, fabricated of a material with thermal expansion complementing that of semiconductor die. Our prototype designs integrating micro heat pipes with Kovar enhance thermal conductivity over that of Kovar alone, thus improving the cooling of microelectronic die.

The new substrates are made with relatively low-cost processes and materials. In volume production, these designs could be made at a cost comparable to that of common substrates such as laminate printed wiring boards, or alumina or silicon multichip module boards.

We envision the use of micro heat pipe substrates initially as replacements for existing heat spreaders. It appears feasible to use them as the substrate core layer supporting electrical interconnects for circuit board-like assemblies. With their plate-like aspect ratios, micro heat pipes would combine the functions of electrical interconnect and heat sink. It also appears feasible to use them in multi-chip module designs. This technology would allow the use of three-dimensional stacked structures, as well as the more common two-dimensional mother board, for higher power applications.

Background: Traditional Methods for Cooling Microelectronics

Previous cooling work has been based on either passive or active cooling techniques. The passive systems use bulk materials to conduct heat through substrates or slugs in microelectronic packages.¹ Historically materials have been chosen that approximately match the CTE of the circuit components, and include materials such as alumina ceramic, Kovar Fe/Ni/Co alloy, and glass fiber epoxy laminates. For higher thermal conductivity, beryllia ceramic has been used despite the toxic nature of the dust. For some applications, where the CTE is not a mechanical reliability issue, sheets of high thermal conductivity copper or aluminum are used. Today's preferred electronic system designs often exceed the thermal density and mechanical reliability limits of these materials.

In response, new families of materials are emerging for these higher waste heat fluxes. For example, multichip modules have been fabricated on silicon wafers, aluminum nitride ceramic, silicon carbide ceramic, and other materials. These are relatively high cost materials and in general the thermal limit of these materials is in the 1-5 W/cm² range. Incremental progress is being made in bulk manufacturing, metallization, cost, and finishing issues leading to expanding markets for all of these materials. Considerable expense has also gone into the manufacture of substrate grade polycrystalline diamond. However, for pieces larger than 1 cm the production cost is about still 100 times too high for market penetration, and the production difficulties are very challenging.

In addition to the bulk materials, small versions of traditional heat pipes have been used to remove heat from localized points to a remote radiator. Traditional long tube heat pipes have the wrong aspect ratio to conform easily to high density electronic assemblies.²

Active systems are the second approach to cooling and are typically characterized by forced convection of air, or a liquid coolant. Fans forcing air to flow around a board or over a metal finned structure in intimate contact with an active device have been the mainstay of system cooling. For the foreseeable future, fan cooled systems will remain in the majority. However, many systems, such as radar and advanced AF&F units when reduced in volume, are of such high density that air flow cooling is not practical.

Active systems using immersion cooling, spray cooling, and pumped convective cooling in microchannels have been used to a limited extent. The primary difficulty of all the active cooling systems is the requirement for pumping the coolant. In the case of air cooling, fans are available that are inexpensive and reliable; however, the heat flux that can be removed is relatively low. For liquid coolant, much higher heat fluxes can be removed; but, the pumps required to circulate the liquid have a limited life span, due to the seals and close tolerance moving parts.

The Micro Heat Pipe Substrate: A New Approach to Cooling

The new approach of embedding micro heat pipes in a substrate provides important advantages over traditional cooling methods.

- In contrast to traditional cooling methods that employ high thermal conductivity solid materials such as polycrystalline diamond or Al/SiC cermets, the new technology permits the use of a variety of substrate materials with desirable physical properties (e.g., machinability, a specific CTE) in addition to high thermal conductivity.
- Unlike active, forced convective cooling systems such as microchannels or sprays, the new technology requires no pumping power or maintenance.
- The micro heat pipes are passive and reliable.
- The new technology places the cooling in closer proximity to the heat source than traditional cooling methods, rendering it better-suited for cooling electronics.

The basic heat pipe substrate geometry is shown in Figure 1. The micro heat pipe is a planar shape with external dimensions similar to those of an ordinary bulk substrate or heat spreader. However, instead of being a uniform tile of material, the substrate is actually two plates of material with an internal volume for cooling. Between the two plates is a micromachined vapor chamber with wall surfaces covered by micro scale features that act as the heat pipe wick. The two plates with wick features on the inner surface are separated by a spacer, sealed along their edges, and charged with the working fluid (methanol). Locally heated areas on the substrate are then cooled by the evaporation of the working fluid. The vapor recondenses at cooler surface regions on the plate inner walls, carrying with it the heat of vaporization. The fluid is replenished by flow drawn by capillary action through the wick features. This closed loop flow requires no pump and consumes no coolant. The micro heat pipe substrate is a closed, passive system.

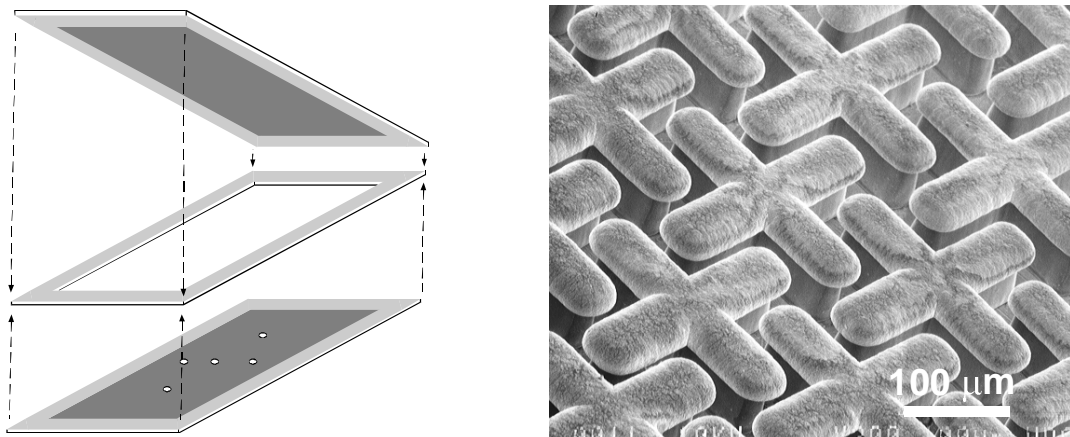


Figure 1. (left) Basic design of the heat pipe substrate: two plates with wick features on their inner surface are separated by spacers and sealed along the edges. (right) Enlargement of heat pipe wick features micromachined on wall surfaces.

Initial work on the micro heat pipe substrates was done using a wall material of silicon.^{3, 4} In those initial designs we used plasma etch and wafer-to-wafer bonding processes for assembly. Silicon did not prove to be a practical wall material, however. Both it and its glass bonding layer were brittle, so the finished product was too fragile for most applications. Also, the processes for etching silicon required extraordinary cleanliness and were too costly. The present work evolved from the silicon effort. We now use a tough material that has a low thermal expansion coefficient; we use potentially low-cost plating processes. Kovar alloy is the current material of choice, although the processes are readily adaptable to other metals as well. Ultimately this approach will permit the manufacture of large-area devices that are mechanically robust and potentially low in cost. The plating processes we developed for use with Kovar can also be used on a silicon wall material to make an improved design over that of the early etched silicon micro heat pipe substrates.

We selected Kovar metal as the substrate wall material because its coefficient of thermal expansion (CTE) matches that of VLSI and GaAs semiconductor die materials. Integrating the micro heat pipes with Kovar significantly increases the effective thermal conductivity over that of Kovar alone. The CTE match helps to maintain low mechanical stresses in a thin rigid bond layer between the die and substrate over the operational temperature range. The thin bond layer contributes to efficient cooling of the electronic die. In addition, the CTE match reduces potential thermo-mechanical fatigue and contributes to high reliability for electronic systems.

This report describes our work to design heat spreaders and develop fabrication processes needed to make micro heat pipe spreaders with metal walls. We describe a test system developed to measure the performance of these devices and discuss a collection of test results. A simple performance-based model using experimentally determined heat transfer coefficients to estimate the performance of the heat pipe is described. We show results from a 3D numerical heat transfer analysis based on this model to evaluate heat spreader applications and compare performance to other bulk material cooling designs. We also discuss the benefits and limitations of the new technology for electronic cooling needs.

Design of Wick Patterns

The use of photolithography to make the heat pipe wick features allows us to design the shape and spacing of the wick patterns to optimize performance. The magnitude of available pumping pressure driven by surface tension forces is related to the spacing between the walls of the wick features. The finer the spacing, the larger the pumping pressure. On the other hand, the drag forces on the liquid increase as the spacing is made finer. This increased drag can limit the rate at which the volume of liquid is returned to the region where it is being depleted by vaporization.

Wick Spacing

We evaluated the magnitude of the pumping pressure for various wick designs during the previous work on silicon substrates. Figure 2 shows four designs we studied with fluid-flow diagnostics to determine liquid drag forces and capillary pumping pressures. These forces were measured using methanol liquid with a method described by Adkins⁵. Table 1 shows

the measured values of permeability and pressure for the four designs, which were etched in silicon to a depth of 55 microns.

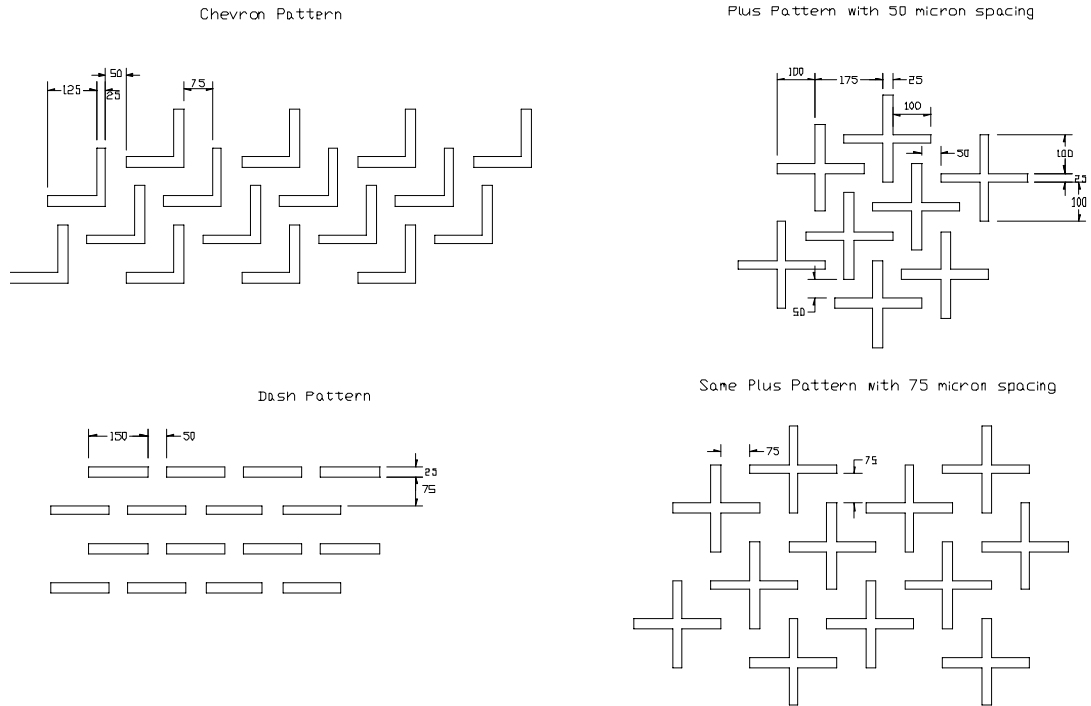


Figure 2. Photoetched patterns used for the silicon substrate testing work. Dimensions are in microns. The features tested were 55 microns tall.

Table 1. Permeability and pumping capacity measured for the four patterns in Figure 2.

pattern/spacing	permeability (μm^2)	peak capillary pumping pressure P(mm H ₂ O)	peak capillary pumping pressure P(Pa)
chevron 75	69	121	1190
plus 50	38.2	135	1320
dash 75	117	112	1100
plus 75	77	110	1080

The shape and layering of the wick features also affect the drag behavior of the fluid through the wick. Figure 1 shows one of the original metal-plated wick designs. This design gives similar pumping performance in orthogonal directions on the plane of the substrate surface. To improve the cooling efficiency, we are developing double layer wick patterns that have a radially converging geometry.

Double Layer Wick Design

This wick design is intended to promote the flow of liquid toward the heat source to replace liquid depleted by evaporation as heat is carried off by the vapor. The wick uses the surface tension on liquid surfaces having a small radii of curvature between the micro scale features to create a pressure gradient that draws liquid back toward the heat source. This flow replenishes liquid depleted by evaporation. A Laplace equation in two dimensions for the confinement and heat input boundary conditions describes the internal liquid flow. For our case in which the heat is dissipated near the center of the spreader and removed at the edges, the liquid flow is close to a radially symmetric pattern. Although one could design the wick pattern with walls aligned to the flow predicted by the Laplace solution, that flow is not sufficiently different from the simple radial flow to justify the additional geometrical complexity at this stage of heat pipe development.

In addition, we decided to develop wicks composed of two layers in an attempt to optimize flow of thick liquid layers far from the heat source and thin liquid layers near the heat source. The first layer adjacent to the substrate wall has the smallest geometrical features spaced about 5 μm laterally and with a height of about 5 μm (see Appendix A wick2 section) and is intended to generate high capillary pumping pressure as the liquid layer becomes thin near the heat source. In typical operation, the liquid layer could dry out in the region under the heat source, causing a loss of heat pipe action. The second or top layer of features has a larger spacing of about 30 μm and wall heights of about 60 μm (see Appendix A wick1 section). The larger spacing is intended to reduce drag of the liquid flow sufficiently far from the heat source where the liquid layer is much thicker. This also maintains a lower liquid surface curvature needed to promote the desired pressure gradient and liquid flow.

The overall wick design is radially symmetric and composed of rectangular and trapezoidal features in plan-view. These are built vertically by Ni electroplating and form walls to produce the radial flow channels. Periodic breaks in these walls allow cross flow of the fluid as necessary to match the pattern of evaporation. As the walls converge radially, one must selectively end some of the walls to maintain the geometry between desired minimum and maximum spacing. While this is a simple design requirement that can be met manually for a few features, when it is applied to greater than 10^5 features in a typical wick design, an automatic layout program is required.

In the program these features are grouped radially and azimuthally. The radial groupings correspond to the radial domains starting with the minimum required azimuthal spacing between adjacent features and extending outward to a point that the azimuthal spacing is just sufficient to allow another set of features to be included while resulting in the minimum required azimuthal spacing. The azimuthal grouping results from the heat pipe symmetry (radial features with a square boundary). This symmetry allows for the wick to be composed of combinations of a single-one eighth section of the square wick surface. The one-eighth section is rotated and reflected to generate the full square pattern. This process reduces the mask file size to effectively one-eighth of what it would be otherwise. Although greater file size reduction could be accomplished with even more complicated

decompositions, this effort was deemed unnecessary. The files from the automatic layout program are used to generate the photomasks for the manufacture of wick prototypes.

Method used to generate mask data to create wick structure

GDSII files are a standard graphics design file format commonly used for photomask design. Computer libraries* that facilitate the layout of circuit geometries in GDSII binary files from a programming environment were developed at Sandia's Compound Semiconductor Research Laboratory (CSRL). This development allows us to manage new mask designs with a parametric database to greatly reduce the effort and turn-around time of initial or iterative design phases of projects. This capability allows us to generate designs for mask art work with large numbers of coupled features that would not be feasible with standard computer aided design using manual placement of features.

The parametric description of mesh designs allows us to evolve designs and to respond to errors such as simple but common miscommunication of complex geometrical ideas. In addition, we have demonstrated that this approach is quite suitably mixed with third party applications providing other design approaches such as manual or scripted layouts using a graphical user interface. Another significant advantage of this approach is that a sophisticated development environment including symbolic and/or visual debugging tools not available in CAD applications can be used to greatly reduce development time.

This programming approach was used to generate masks for the nickel wick designs tested in this effort. Appendix A gives the full parametric representation of the wick design. The following is an excerpt from the appendix of the "wick1" section:

```
// wick1
wick1Width= 20.0;// (µm)
wick1Spacing= 30.0;// (µm)
wick1Mark= 200.0;// (µm)
wick1Space= 25.0;// (µm)
wick1ExtWidthMin= 5.0;// (µm).
```

The radial walls are composed of rectangular sections separated by radially alternating gaps. The parameter wick1Width is the lateral wall width; wick1Spacing is the minimum lateral azimuthal spacing between the walls. The parameter wick1Mark is the nominal radial run between the gaps with widths given by wick1Space. The wick1ExtWidthMin is the minimum width of extension features used to cross radial zone boundaries. This section is quite representative of how geometrically defined parametric databases can be used to generate mask art work.

The left side of Figure 3 shows the geometry that results from scaling the wick1 and wick2 parameters given in Appendix A by a factor of 32 larger so the features can be seen on paper. Notice the gaps in the walls of the image. These gaps are intended to cross flow,

* For detailed information, contact Chris P. Tigges in Org. 01713 at Sandia National Laboratories.

thus preventing heat pipe channels from being blocked by particle contamination during operation. The right side of Figure 3 shows a magnified view of a one-eighth section of the corresponding finer featured lower wick 2. In this lower layer, four radial groups are evident. No gaps in the radial walls were used in this layer, which is typically only 5 μm thick compared to 60 μm thickness for the wick 1 layer. Note also that there are extensions of the wick 2 fences (rectangular and trapezoidal) near radial zone boundaries. These extensions were added to the second generation of wicks to streamline the flow.

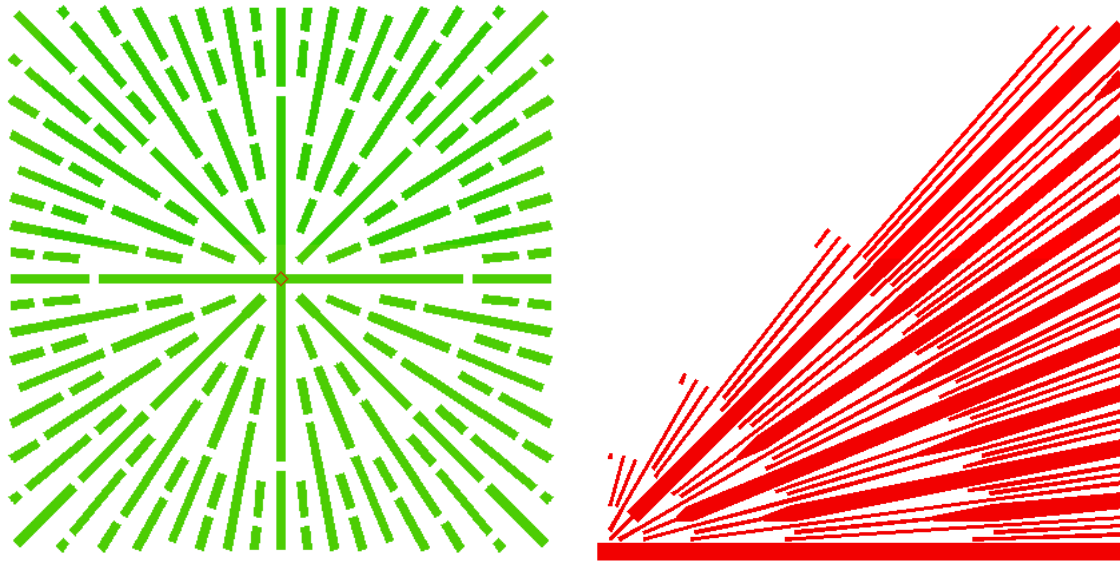


Figure 3. (left) Wick 1 layer (upper layer) resulting from scaling parameters 32x actual used values. This wick is intended for the thick flow regions of the heat pipe. (right) One octant of the wick 2 layer (lower layer) again at 32x normal scaling. Having finer features than wick 1, wick 2 is expected to enhance the flow where the fluid layer is thin and approaching the dry out stage.

Conversion of parametric data to CAD data for mask manufacture

The parameters described above are used with the GDSII library interface to generate a binary data file describing the photomask geometry. The resulting GDSII binary file is about 2 megabytes in size and quite practical for mask production. This file is transmitted to a commercial mask production company, and the resulting photomask on a glass substrate is used for the contact printing of Kovar prototype wick parts.

Figure 4 shows the result of the mask design process at higher magnification. This view is for a location some distance from the center at a transition point where a new set of walls are added to the pattern to keep the spacing within the selected range. The top or outermost layer is shown in the top figure. Here one can see the gaps are staggered so that gaps occur at only one side of a flow channel at a time. The lower part of Figure 4 shows the two layers superimposed. The layer that is plated adjacent to the substrate wall has the fine (5 mm wide) features.

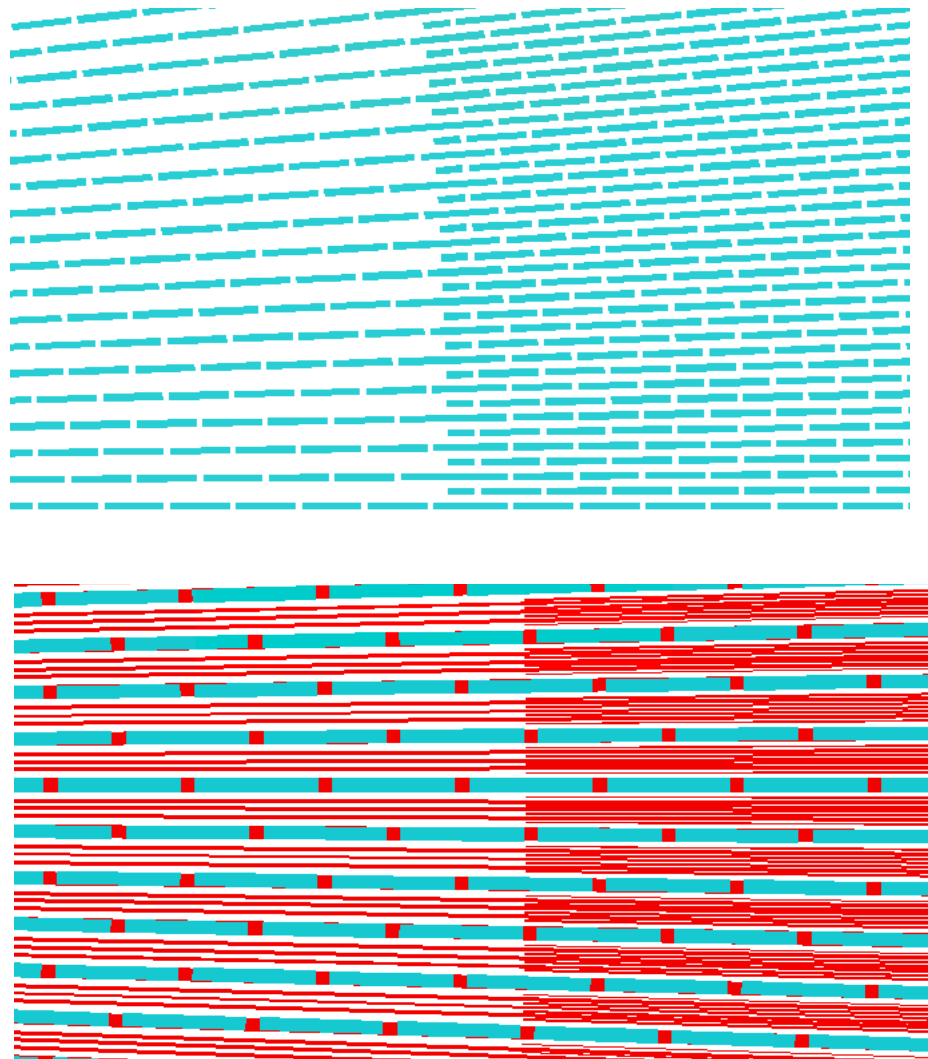


Figure 4. (top) Wick 1 layer detail. (bottom) Similar detail including both wick layers. Both details are near a radial zone boundary. Compare with SEM details in Figure 5.

Figure 5 shows an SEM photo of the parts made from masks similar to those of Figure 4. The left side shows a converging pattern near the center of the substrate wall. The open circular area in this figure is provided on the part to allow a spacer disk to be welded between the two heat pipe walls to increase strength and rigidity of the finished heat pipe. The right side of Figure 5 shows a magnified view of the wick features. Note the first layer of fine features in addition to the taller second layer. The features on the second layer were overlaid in this part to give additional confinement to the liquid and to form corners that would aid in producing additional meniscus surfaces on the liquid.

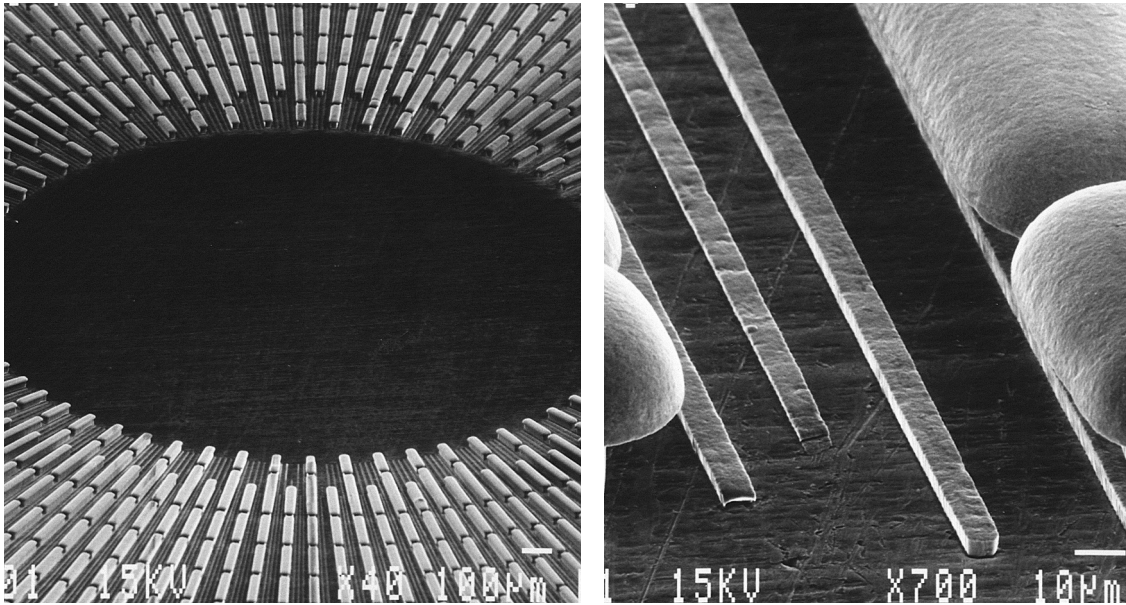


Figure 5. (left) SEM detail of center of heat pipe wick. (right) SEM detail near radial zone boundary clearly showing the two wick layers. The top wick layer has been overplated, providing additional height and corners. Compare SEM details with the mask design in Figure 4.

Photo Lithography and Plating Processes

This section describes the processes used to generate the wick features on the interior surfaces of the micro heat pipe. The photo masks described in the previous section are used in this process to photographically define the features in a resist layer that is then developed. The open areas of the developed photo resist layer are filled with metal to make the finished wick features seen in Figure 5. Two sequential processes are used to make the stacked pair of layers seen in this design.

A list of the processing steps is given in Appendix B and will be further described here. Although simple in principle, these processes consumed the largest fraction of the resources and time spent in developing the micro heat pipe technology. Means to streamline this part of the process are needed to improve the viability of this technology. In spite of significant effort, the current facility used for this work was unable to develop wick feature taller than about 60 μm . Although this is a significant accomplishment, the development of high performance heat pipe designs will require additional work to improve this limitation on pattern height.

We now discuss several parts of the process used to prepare the wall materials, apply the photo resist, optically expose and develop the resist, electro plate the metal features, and remove the remaining resist material.

Cleaning: Kovar wafer preparation and cleaning is a critical component of the fabrication process. It is important that the incoming wafers be round and as flat as possible. Kovar

wafers with a three-inch diameter have been used throughout this process. These were prepared from rolled Kovar sheets and flattened to less than 50 μm . These wafers need to be first cleaned with trichlorethylene, followed by rinses in acetone and isopropanol. The next operation is a 15-minute sputter cleaning process with an argon-ion sputter gun, using the standard CSRL conditions.

First Layer Channels: The ultimate result of this sequence of operations is thousands of features, which are 5 micrometers wide and 5 micrometers tall, patterned in electroplated nickel. In order to accomplish this process, AZ 4620 photoresist^{*} is spun at 2000 rpm for 30 seconds. This yields 8 microns of resist. It is then baked at 90°C for 2 minutes on a hot plate. It is exposed using the first layer channel mask to 350 millijoules of energy on an MA-6 Suss contact printer.[†] The pattern is then developed in AZ 421K developer diluted 4:1 for 140 seconds. The wafer is then nickel plated in Selrex nickel sulfamate plating solution[‡] using a custom-made fountain plating system. The wafer is DC plated for 36 amp-minutes for a 4.3x4.3 cm (1.7x1.7 inch) square mask area. The plated area of this first channel layer is 1.5 sq. in. This produces a film about 5 micrometers thick. The photoresist is stripped in acetone, followed by an isopropanol rinse.

Second Layer Channels: This sequence of operations produces 60 micrometer tall mushroom-shaped nickel features on top of some of the first layer channels. Several lithographic procedures have been tried to accomplish this. AZ4903 photoresist was initially tried as a nickel plating mask. It exhibited poor adhesion to Kovar and lifted during electroplating. SU-8 photoresist[§] was tried next. It has excellent adhesion to Kovar but can only be removed after electroplating by using long plasma stripping procedures. These long exposures to oxygen plasma damaged the surface of the nickel and Kovar, sometimes causing delamination of the nickel.

Successful processing of the 60 micrometer tall features was done with AZ 4620 photoresist spun on top of the first plated layer at 900 rpm for 20 seconds. The wafer is baked for 6 minutes at 90°C. It is allowed to cool for 2 minutes. It is then recoated with a second layer of AZ 4620 following the same spin procedure as above. The total of two spins produces a resist thickness of about 55 microns. The wafer is then exposed on the MA-6 contact printer for a total of 2560 millijoules of energy. The wafer is then developed in AZ421K developer diluted 1:4 for 135 seconds. Immediately before plating, the wafer is dipped into a 1000:1 water/Triton X-100 solution. The wafer is agitated until all bubbles are removed. The wetted wafer is placed immediately into the electroplating apparatus without drying. This step is very important to prevent bubble formation that interferes with electroplating. The same fountain plater and solution are used to plate the second layer, but with an important variation. It was observed that 50% non-uniformity in height of the plated layer across the plated surface occurred with this plating bath when the power supply is used in DC mode. The nickel plating is thicker at the edges of the wafer. Several improvements have been made to make the plating more uniform. The first improvement

^{*}AZ Corporation, a division of American Hoechst

[†]Karl Suss America Corp

[‡]Enthone OMI

[§]Microolithography Chemical Corp, 1254 Chestnut St., Newton, MA.

was to change the counter-electrode from a 2-inch square nickel sheet to a titanium basket filled with large (~0.5 cm dia.) nickel spheres. This large counter electrode helps to straighten the electric field lines. The second improvement was to use pulsed-DC plating. The formula chosen for plating is a compromise between uniformity and plating speed. If a 1:10 pulse plating cycle is used, the plating is very uniform but extremely slow. It was found that adjusting the ratio of 3:7 (3 plate: 7 de-plate) produced plating rates of about 1 micron/minute. The initial current adjustment was 6 amps at DC (non-pulse). Plating total was 480 amp-minutes across the 3.4x3.4 cm square mask patterned area. The plated area of the second layer is 0.6 sq. in.

Post-Plating Process: After electroplating, the resist was stripped using acetone, followed by alcohol rinses. An important step after this stripping process is surface preparation. It was found that an oxygen plasma makes the nickel surface more wettable than for a surface from only solvent stripping. A 15 minute treatment in a high-density (electron cyclotron resonance) oxygen plasma containing 8% carbon tetrafluoride (CF₄) removes any organic traces remaining after the solvent stripping process and oxidizes the nickel slightly to make it more hydrophilic. A good test of wettability after this procedure is if a drop of water is placed at the center of the pattern after this treatment, it rapidly spreads evenly out to the edges.

The Nickel Fountain Plating Equipment: This plating equipment is a custom built system made using an 8 inch CPVC cube with a drain at the bottom. A sketch of this system is shown in Figure 6. Inside this cube is a 5 inch round CPVC pipe on top of which rests a CPVC wafer holder. The wafer is attached face-down to this holder with piano-wire spring clips. The clips also serve as electrical connection to the wafer. Sulfamex Make-Up nickel plating solution* is pumped from a sump through a filter using a peristaltic pump with a pumping rate of 7.6 liters/min. No plating solution comes into contact with any metal surfaces. This solution is pumped up the 5 inch pipe and onto the face of the wafer. The solution moves across the wafer and falls into the cube, where it is returned to the sump. The power for electroplating is supplied by a DUP10-1-3 pulse plating power supply.†

Previous Electroplating Work on Silicon and Kovar: Some of our early process development work was done by plating metal features on silicon substrates. Electroplating either nickel or gold on silicon was accomplished using a titanium (500Å) and gold (3000Å) seed layer. After plating, the seed layer was stripped in KI₃ solution. The titanium was stripped in 10:1 HF. These produced good patterns with limited feature height, but interest in the Kovar designs kept us from pursuing this wall material to a finished heat pipe design.

* Enthone OMI

† Dynatronix Corp

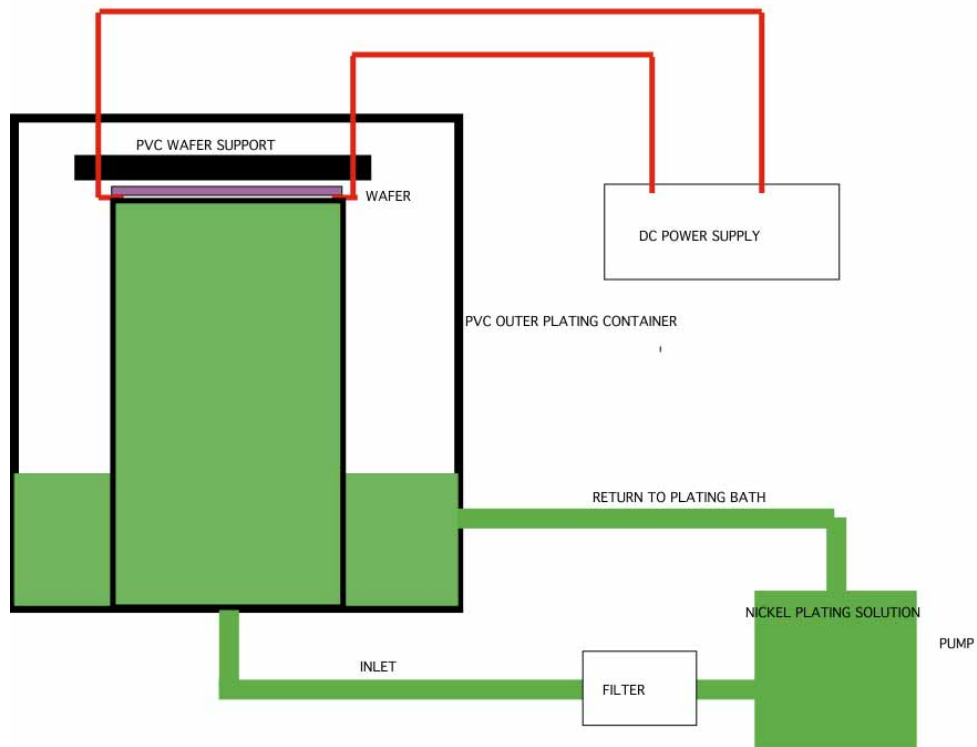


Figure 6. Diagram of the fountain plating system used for the nickel wick deposition.

Initially, a Ti/Au plating base as above was used on Kovar to promote adhesion to the substrate. It was later found that using trichloroethylene as a solvent clean, followed by an argon sputter prior to plating provided good adhesion of nickel directly to Kovar. Thus this seed layer was not used in the later Kovar processing.

Present and Ultimate Limits of Wick Sizes: The thickness of features made with the current technology is limited. At present, 5 micron lines and spaces are patterned directly on Kovar wafers, then electroplated 5 microns thick. A second pattern of resist is plated above the first pattern. The second is aligned to within 2 micrometers of the first pattern, and is plated to about 70 micrometers. Future resist technology may allow a third layer of resist and plating to yield over 100 microns of nickel pattern height. Six-inch wafer plating may become available, such that larger micro heat pipe substrates or multiple devices could be put on one wafer. It is possible to electroplate on other non-oxide forming surfaces such as copper, but not on aluminum, which forms a surface oxide.

Additional work is under way to develop a commercial source of supply for wick production that would reduce cost and improve availability of these devices for new applications.

Heat Pipe Materials and Assembly

Background

Materials

As described in earlier sections, the metal micro heat pipe requires a material with a coefficient of thermal expansion which closely matches the thermal expansion of silicon over the operating temperature range of the integrated circuitry. Availability and ease of fabrication are also important considerations. The alloy selected for the current designs is Kovar, which is an iron-nickel-cobalt alloy originally developed for glass/metal sealing applications. The alloy has been used for making hermetic seals with a variety of glasses and ceramic materials, and has been widely used in power tubes, microwave tubes, transistors, and diodes. In integrated circuit manufacture, the alloy has been used for flat pack and dual-in-line package construction.

The alloy is designated by two ASTM Specifications, F-15 and F-1466. ASTM F-15 covers the conventional Kovar alloy, while the ASTM F-1466 Specification was developed to provide improved brazability through stringent control of residual element limits. Material is currently produced to both specifications, although the cost and availability of material produced to the F-15 Specification are generally more favorable than for material produced to F-1466. The chemical requirements for ASTM F-15 Kovar are shown in Table 2. All heat pipes fabricated in the current work were produced from conventional F-15 material in the mill annealed condition.

Table 2. ASTM Chemical Requirements for Kovar Alloy.

Element	Composition (wt%)
Iron, nominal	53
Nickel, nominal	29
Cobalt, nominal	17
Manganese, max	0.50
Silicon, max	0.20
Carbon, max	0.04
Aluminum, max	0.10
Magnesium, max	0.10
Zirconium, max	0.10
Titanium, max	0.10
Copper, max	0.20
Chromium, max	0.20
Molybdenum, max	0.20

Kovar Fabrication Characteristics

The fabrication characteristics of Kovar are relatively well known, although there are several important considerations which will be briefly reviewed here. The ductility of annealed Kovar is sufficient (approximately 30% elongation) to accommodate complex cold forming operations, so that non-planar shapes should be readily producible. However, as a result of its austenitic structure and high work hardening rates, tooling for forming operations probably requires careful design to allow for spring back.

The machinability of Kovar can best be described as poor to moderate, and is generally similar to that of austenitic stainless steel (e.g. 304 or 316 stainless steels). These difficulties arise from the high ductility and work hardening characteristics of the alloy, which result in poor chip formation during cutting operations. Dry machining, such as might be required to produce penetrations into the heat pipe cavity, is feasible, but is also relatively difficult from the perspective of mass production and tool life. Kovar is readily amenable to electro-discharge machining (EDM).

The weldability of Kovar is similar, albeit somewhat inferior to, that of austenitic stainless steels like 304L or 316 [Ref 6]. The alloy can be welded by essentially all conventional processes, including arc, laser, and resistance welding. The feasibility of direct joining of Kovar to copper, such as that evaluated in the current work, has not been specifically documented in the literature. Direct Kovar to copper transitions are common, however, in the roll bonding of sheet materials to produce the Tri-Clad layered material. Resistance welding of copper to Kovar, though difficult, is feasible and was also evaluated in this work.

The solderability of Kovar is comparatively difficult because of the oxides which form on its surface. Direct soldering of this alloy normally requires the use of aggressive fluxes which are difficult to remove. The possibility of introducing soldering fluxes into the heat pipe cavity, and the difficulties associated with removing these fluxes was felt to preclude their use in this application. Thus, solderable Ni/Au plating was evaluated for the micro heat pipe solder joints. In this approach, a solderable metallic nickel layer is first deposited and then, without removal from the evaporation or sputtering equipment, a protective gold layer is deposited on the nickel. During soldering, the gold layer is dissolved by the molten solder which then wets the nickel surface. Although somewhat complex, this is a relatively standard procedure in microelectronics packaging and should be applicable to large scale production.

Heat Pipe Fabrication Requirements

The nature of potential micro heat pipe applications (i.e. high volume, low cost) placed several constraints on the fabrication processes evaluated in this work. Specifically, it was desired that the processes be widely available, well characterized, and robust. In addition, it was desired that the processes be amenable to mass production and reliable. Thus, although the primary goal was to provide assembled heat pipes for thermal testing, a secondary goal was to assess processes and procedures which might be adapted to mass production or might provide for more reliable operation. For these reasons, conventional processes such as laser and resistance welding were used. This is not intended to imply that

process development was not required, however. For example, the laser and resistance weld schedules were developed through processing trials on test parts which were geometrically similar to the current heat pipe design. Other processes such as alternative means for attaching the fill tubes were also evaluated but not used for the production of test assemblies.

Fabrication Procedures

Piece Part Fabrication

Heat pipe wick assemblies were fabricated on 0.020" thick Kovar sheet. To facilitate photolithography, the sheets were machined into 3" diameter wafers by EDM (in an effort to maintain the flatness of the sheet). In order to make the Kovar wafers as similar as possible to typical silicon wafers, initial parts were polished on one side by abrasive methods using an alumina polishing slurry. However, relatively severe curvature of the wafer resulted from the polishing, apparently because of residual stresses within the rolled sheet. Subsequent photolithography trials indicated that polished surfaces were not required for wick fabrication. Final cleaning and preparation of the wafers was therefore accomplished by manual scrubbing with fine (3/0) abrasive sponges and an Alconox/water mixture. The parts were then rinsed in water and finally in ethanol. Following deposition of the wicks, the wafers were cut into 1.9" squares by using a conventional diamond wafering saw.

The internal supports and spacing frames (initial designs used internal supports which were integral with the frame) were machined from either 0.010 or 0.020" thick Kovar sheet by EDM. In an effort to minimize the incorporation of impurities into the closure and support welds, molybdenum wire (rather than brass) was used in all EDM operations. Figure 7 shows the initial frame design with integral internal supports, and Figure 8 shows the frame design used in later heat pipes. Internal supports for the latter designs consisted of 0.1" diameter Kovar disks which were also produced by EDM from the sheet material.

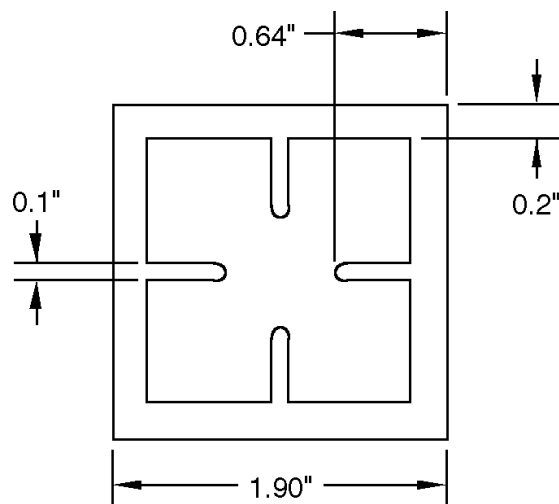


Figure 7. Initial frame design with integral supports. Dimensions are nominal.

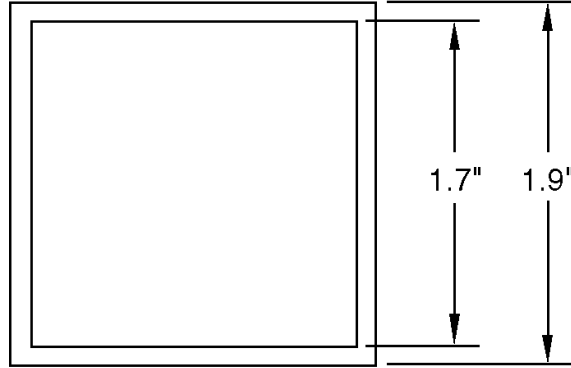


Figure 8. Frame design used in latter heat pipes. Dimensions are nominal.

Heat pipes fabricated in this study used one-piece frames to facilitate assembly. For large scale production, however, this would likely be an inefficient use of material. It should be noted that a two-piece frame (cut at diagonal corners) could easily be substituted, and would allow for near 100% material utilization. Further, it is believed that EDM procedures need not be used for piece part fabrication, and that stamping could be used to produce piece parts of sufficient dimensional accuracy and in high volume. Piece parts were cleaned using the same manual abrasive cleaning described above. This cleaning procedure is also not amenable to large numbers of parts, but it is believed that suitable chemical cleaning procedures could be developed for use in high volume production.

Assembly and Welding Procedures

Assembly of the heat pipe includes several major operations and can be visualized with the aid of Figure 9. These operations include: (1) laser drilling of the fill port hole in one wick plate; (2) resistance welding of the internal supports to one wick plate; (3) assembly and laser tack welding of wick plates to the spacer frame; (4) laser seam welding of the assembly edges; (5) resistance welding of internal supports to the opposite wick plate; (6) leak testing; (7) bead blasting and Ni/Au plating; and (8) solder attachment of the fill tube. The specific concerns and welding parameters associated with each of these operations are given below.

The fill port hole (0.040" diameter) was drilled by using a Lumonics JK 704 400 watt pulsed Nd:YAG laser under the following conditions:

2 ms pulse at 20 Hz (LD2 mode)
165 Watts
8.5 Joules
Air assist at 50 psi
Sharp focus

These conditions produced an approximately straight side wall in the hole, with a minimum of spatter (which could potentially damage the wick surfaces).

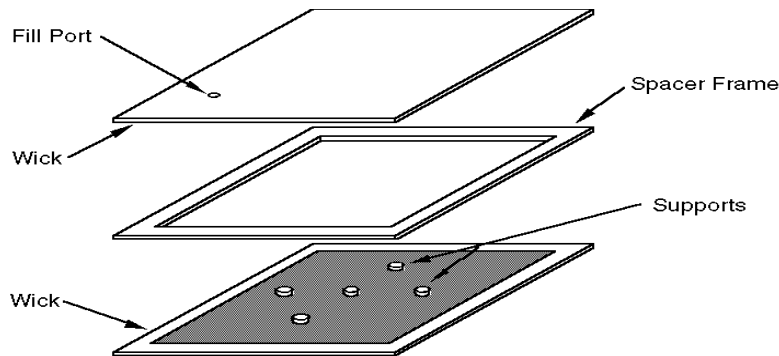


Figure 9. Schematic diagram of heat pipe assembly

Resistance welding of the internal spacers was evaluated by a parametric study of the welding parameters coupled with metallographic analysis to determine the most suitable conditions. For the initial support attachment, a UNITEK 250DP resistance welder and the parameters in Table 3 were used:

Table 3. Resistance weld parameters for UNITEK 250DP welder.

<u>0.010" Thick Support</u>	<u>0.020" Thick Support</u>
0.060" dia. Cu electrodes	0.060" dia. Cu electrodes
medium pulse	medium pulse
polarity (+)	polarity (+)
pressure: 9 lbs	pressure: 9 lbs
87.5 Wsec	95 Wsec

These parameters produced a weld zone approximately 0.032" in diameter; a typical cross section (for a 0.010" thick support) is shown in Figure 10. It should also be noted the internal supports in several of the initial heat pipes were attached by laser piercing welds from the outside of the wick plate. This procedure could not consistently produce welds of adequate strength, however, and was therefore abandoned.

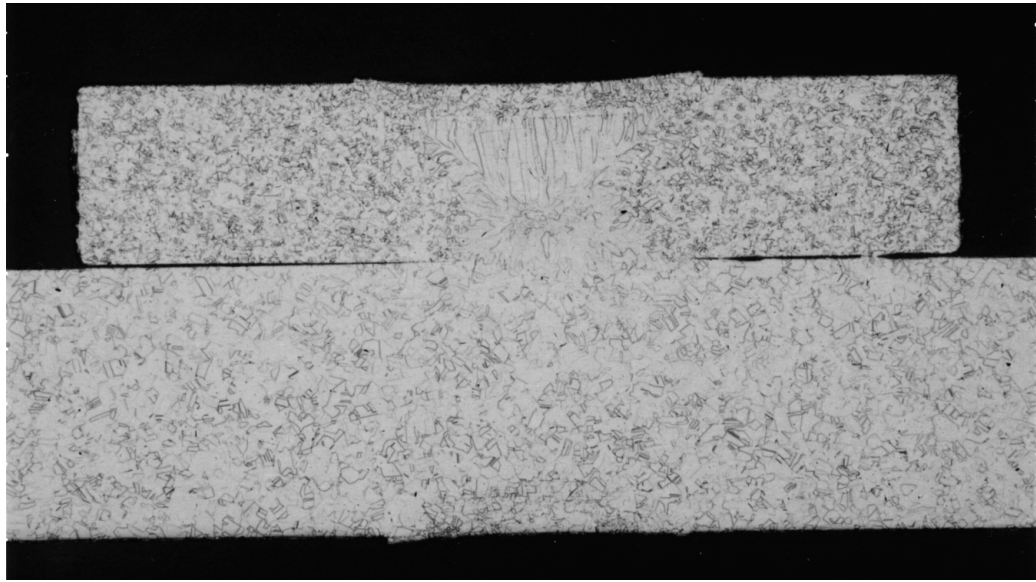


Figure 10. Cross section of first internal spacer resistance weld.

For the closure welds, the assembly was held in a smooth jawed vise and tack welded at eight places (two per side) on the outer perimeter. For the tack welds and final seam welds, a Lumonics JK 704 Nd:YAG laser operating under the conditions in Table 4 was used.

Table 4. Weld parameters for Lumonics JK 704 Nd:YAG laser welder. These welds attached the front and back sides of the heat pipe substrate to make the hermetically sealed assembly.

Tack Welds	Seam Welds
3 msec pulse	3 msec pulse at 20 Hz
166 watts	160 W average power
8.2 joule	8.1 J/pulse
Focus: +0.050	+0.030" (above surface) focus
Argon cover gas	Argon cover gas
	10 inches per minute

A typical cross section of the closure weld is shown in Figure 11. The penetration for these welds is approximately 0.016 in. Cracking problems were not encountered, probably because of the very low restraint associated with the edge weld geometry. For the thicker spacer frames, two weld passes were used on each edge to insure joint integrity along both weld junctions. Although it was not quantitatively evaluated, the overall flat-

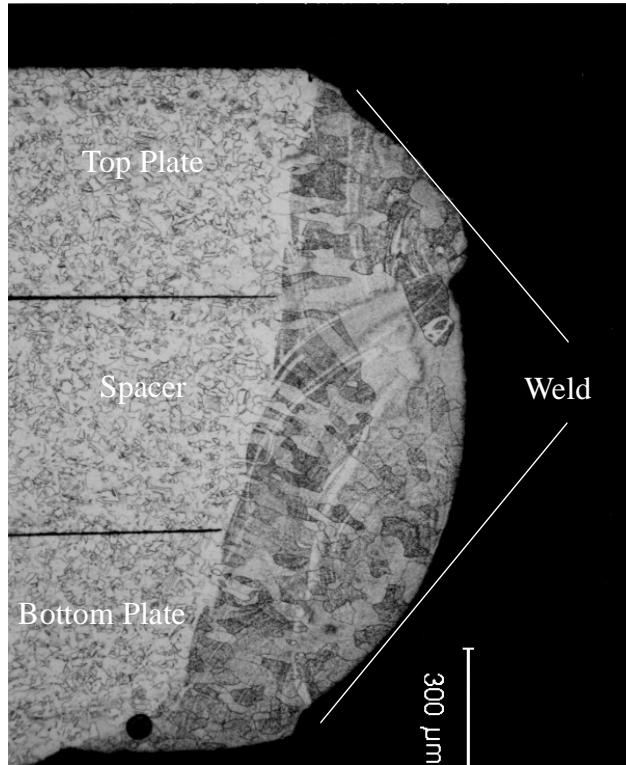


Figure 11. Cross section of closure weld at the edge of the heat pipe substrate. Note that the weld melt zone spans the entire thickness of the substrate.

ness of the welded assemblies appeared to be acceptable.

Final processing included resistance welding of the internal support to the second wick plate. This was accomplished by using a procedure similar to that used to attach the support initially. For these welds the parameters were identical to the initial resistance welds, except that 130 W-sec energy was used. A typical metallographic cross section at the internal support is shown in Figure 12. The heat pipes were then laser scribed with an appropriate designation and helium leak tested.

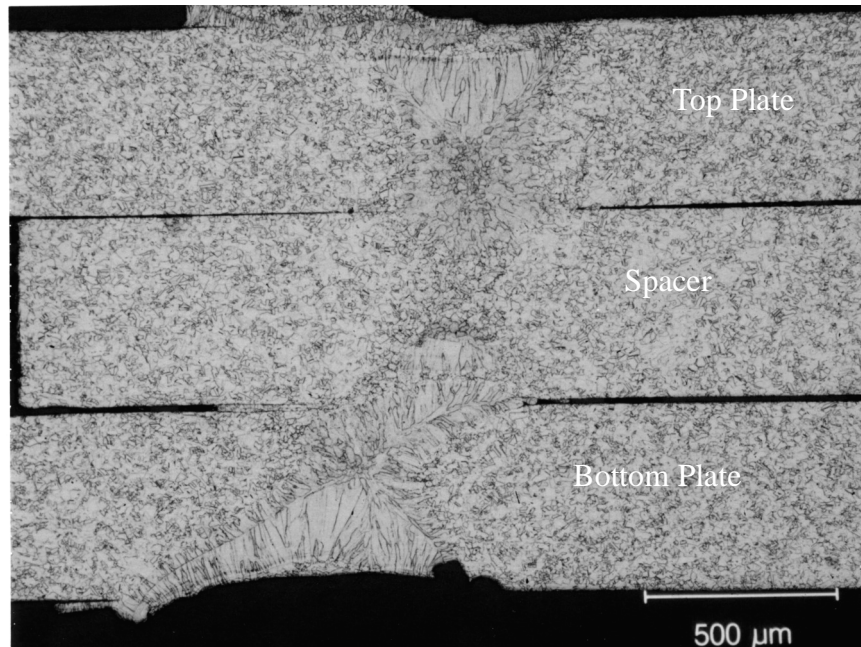


Figure 12. Cross section of second internal support resistance weld.

Assembled heat pipes were then Ni/Au plated to improve solderability and to protect the surfaces from atmospheric corrosion. The nickel and gold were electron beam evaporation coated using conventional procedures to thicknesses 0.195 and 0.127 microns respectively.

The copper fill tube was then attached by using a brass fitting and a two step soldering procedure. Figure 13 shows the fitting and copper tube as attached to the wall of the metal heat pipe. To aid in the later pinch off sealing process, the copper tube is in a softened or fully annealed state obtained by treating it in a vacuum furnace at 600°C for 1 hour. The copper tube is soldered first to the fitting with a solder having melt temperature of 221°C.* Next a layer of ribbon solder[†] with a melt temperature of 181°C is used to attach to the plated Kovar surface. A ph neutral water soluble rework flux[‡] is used with these solders.

*Indalloy #121, Indium Corporation of America.

†Indalloy #205

‡#2331-ZX, Kester Solder Co., Des Plaines, IL.

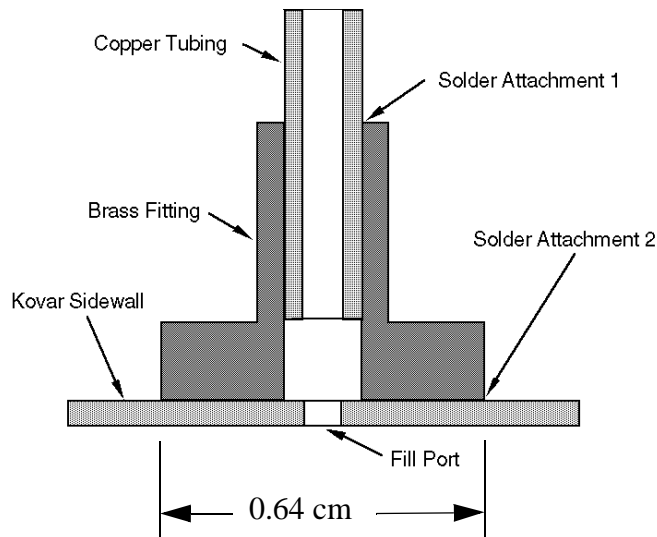


Figure 13. Schematic diagram of fill tube attachment to the heat pipe wall.

Alternate Fill Tube Configurations.

The method used for attachment of the copper fill tube, though suitable for the test prototypes, is not considered suitable for most realistic heat pipe applications. This is because the fill tube/fitting design takes up a significant amount of area on one face of the heat pipe, restricts the ability to locate heat pipes close together, and is relatively delicate from a mechanical perspective. As a result, several alternative filling attachment designs were evaluated.

Since the filling system is currently based on a copper tube pinch-off for final closure, the designs were limited to those which incorporate a copper pinch tube. The major requirements for the alternative fill tube designs were that they attach at the edge of the heat pipe, exhibit appropriate leak integrity, and have sufficient mechanical strength to survive pinch-off and moderate handling. In addition, it was desired that the proposed designs have at least a reasonable potential for application in a mass production environment.

Two basic joint types were evaluated, including a direct solder seal and a copper to Kovar percussive arc weld. The joints were evaluated on subsize heat pipe mock-ups similar to that shown in Figure 14. These mock-ups were 0.7" on each side and had a spacer frame with a 0.5" diameter hole on the inside, which produced a configuration (on the center of each side) similar to that in the actual heat pipes. The laser welding procedures were identical to that used for the heat pipes, and the mock-ups also contained a hole on one face to facilitate helium leak testing.

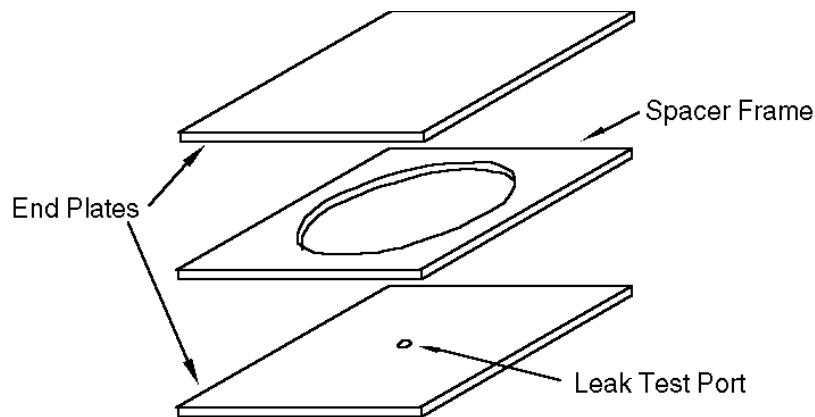


Figure 14. Mock-up of heat pipe used for fill tube attachment trials.

Direct Solder Attachment

The fabrication of a direct solder connection between the copper pinch-off tube and Kovar heat pipe is complicated in that a simple cantilever connection between the end of the pinch-off tube and the heat pipe edge would have insufficient strength, so that some type of tube and socket joint is required. It is further complicated by the poor solderability of Kovar and the potential problems associated with the removal of solder flux from the heat pipe cavity. As described earlier, a common method for overcoming the solderability problem is to create a more solderable surface by Ni/Au plating, which, in the case of the heat pipe must be done by vacuum evaporation or sputtering to avoid contamination of the interior of the pipe. Unfortunately, this approach is incompatible with the tube and socket joint because of the difficulty of plating the interior of high aspect ratio small holes.

Thus, a compromise must be reached amidst the constraints of solderability, mechanical strength, and vacuum plating. Such a compromise joint is shown in Figure 15. The design retains the mechanical reinforcement of a conventional socket joint but incorporates additional lines of sight for the plating operations. For the tests joints fabricated in this work, the nickel and gold were applied by DC sputtering with RF bias (in attempt to further improve the coating of the joint side wall) to 0.195 and 0.127 microns, respectively. Soldering was conducted in a manner similar to that used for the conventional fitting design. Of four test joints produced with this design, however, only one showed reasonable leak performance.

There are several shortcomings with the direct solder attachment. First, in order to maintain cleanliness within the heat pipe cavity, the joint must be machined without the use of lubricants. For Kovar, which has relatively poor machinability, it is difficult to maintain tight tolerances in the counter-bore, and deburring of the intersection of the counter-bore and plate surface is critical. As a result, the ability to produce this joint reliably for large numbers of parts is suspect. Secondly, the primary sealing surface for the joint (see Figure 15) is relatively small, so that the seal length is also small. Finally, the

soldering operation is difficult, and because the protective gold is dissolved during the operation, rework of poor solder joints is problematic. Thus, although the trial joints indicate that the direct solder attachment has some merit and appears feasible (with some additional development), it is not believed to be a generally useful approach.

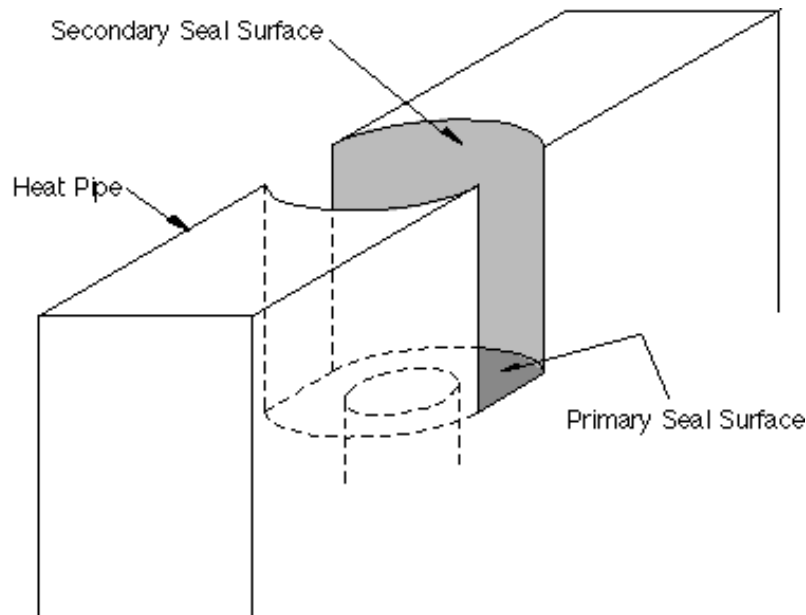


Figure 15. Diagram of direct solder seal joint.

Percussive Arc Welding Attachment

The geometry of the heat pipe and tube lends itself to a direct joint between the copper and Kovar. For this type of attachment, the most suitable welding process is percussive arc welding. In this welding procedure an arc (powered by a capacitor discharge) is established between the two parts to be joined, while at the same time, the parts are mechanically driven together. This process is very common (it is very similar to capacitor discharge or stud welding) and is used to make attachments as diverse as screw stud attachments to bridge decking, wire attachments to large surfaces, and earring posts.

The mock-up heat pipe assembly was prepared by milling a small flat (about 0.065" across) on one edge to remove the surface contour and roughness left by the laser welding, then drilling a 0.030" hole 0.10" deep into the heat pipe cavity. Note that this joint preparation is similar to that used for the direct solder attachment, Figure 15, except that no counter-bore was used. A section of copper tube approximately 0.5" long was cut using a razor blade (rolling it on a tabletop leaves a finished end like a tubing cutter), and one end was finished using a small countersink. This procedure thinned the wall of the tube from the ID toward the OD at a sixty degree angle and was intended to reduce the tendency to plug the hole during welding. The opening was not cut to a full knife edge, as it would tend to produce some flaring of the tube end.

An EFD Model 2200 percussive arc welder was used for the weld trials and was operated using the following parameters:

Capacitor bank A (1400 mfd) - setting #2 (2800 mfd)

Capacitor bank B (2500 mfd) - setting #2 (5000 mfd)

Total = 7800 mfd

Voltage: 75 V

Weld Control (controls speed of gap closure) set at 72 psi.

Collet stop was set at one sixteenth of an inch.

Tube was extended one quarter of an inch out of the collet.

Polarity: Reversed (copper tube ground)

The Kovar sample was held in a copper fixture so that the edge was aligned with the axis of the tube (this fixture was placed on a thin alumina sheet to insulate it from the rest of the welder). The tube was aligned with the hole drilled in the Kovar and the weld was then made.

A macro photograph of a trial weld is shown in Figure 16, and a metallographic cross section of the weld is shown in Figure 17. In the unetched condition, Figure 17(a), it is apparent that some porosity was formed in the joint area (note that the weld appears separated in Figure 17(b), but this is due to attack of the weld metal by the etchant used). Additional weld procedure development should be capable of reducing the weld porosity.

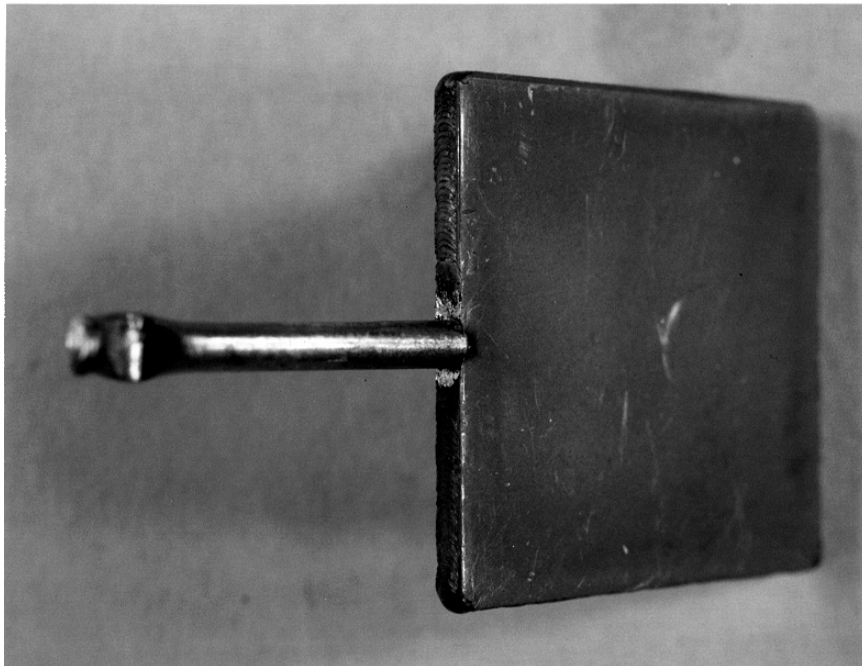


Figure 16. Macro photograph of percussive arc weld tube attachment.

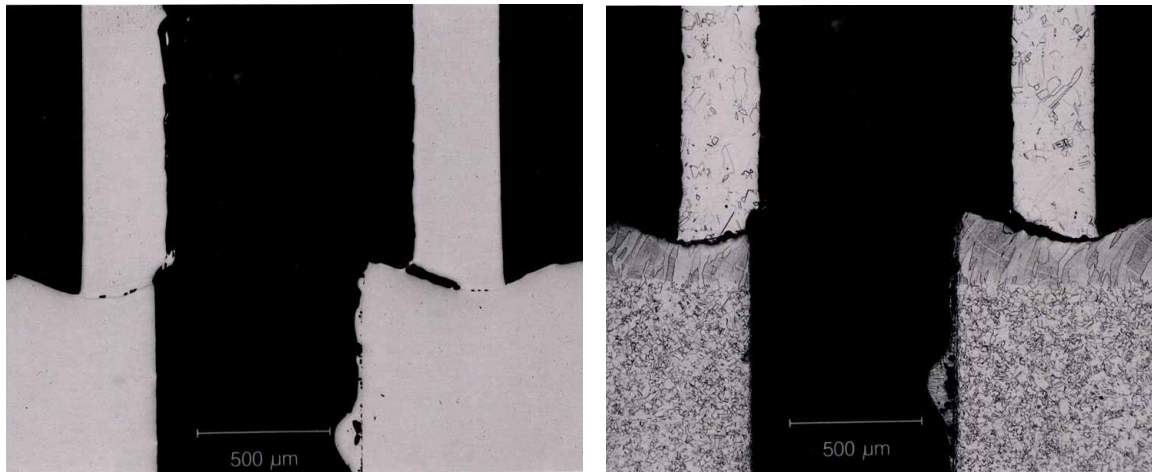


Figure 17. Cross sections of percussive arc weld: unetched (left), etched (right).

As shown, the joints appear to be reasonably well bonded, although maintaining alignment of the tube was found to be somewhat problematic. It is believed, however, that this difficulty should be simple to correct through appropriate fixture design. The potential seal length for the percussive arc welds is relatively short (approximately equal to the tubing wall thickness), but since the weld joint is likely to be significantly stronger than that for a solder joint, this is not thought to be a major source of concern. Helium leak testing of four percussive arc welds indicated that acceptable attachments can be made by this procedure. In addition, simple mechanical examination of the joints indicated that the copper tube could be bent approximately 45° before failure of the joint, and this implies that the joints should be resistant to moderate handling and deformation. Machining requirements, though similar to those used for the solder attachment, are less stringent in terms of dimensional tolerances. A small counter-bore would also aid in alignment and would probably improve mechanical performance. Finally, the percussive arc welding process is amenable to high volume production, and it should be possible to rework faulty joints without affecting heat pipe performance.

It should be noted that only a minimal amount of weld schedule optimization was conducted for the percussive arc welding attachment. Moreover, no attempt was made to optimize the end preparation of the copper tubing prior to welding. Nevertheless, these initial results are very promising in that relatively robust and leak free joints were produced. It is therefore believed that, when optimized to reduce the tendency for pore formation, the direct attachment of the pinch-off tube should provide a suitable means for heat pipe closure.

Coolant fill process

To activate the heat pipe spreader, one must fill a fraction of the internal volume of the heat pipe without introducing air or other noncondensable gas to the interior of the heat pipe cavity. A custom vacuum pump and fill manifold system was developed for this purpose.

A mechanical roughing pump and liquid nitrogen cold trap was used as the pumping source. This system had valve and reservoir chambers to allow the interior of the heat pipe to be evacuated to pressures below 10 millitorr and to then introduce methanol liquid through the pump out tube to completely fill the heat pipe volume with coolant. Typically each pipe was filled and completely pumped out two or three times prior to the final filling to help clean the interior surfaces from any remaining contaminants.

A metering process was used to establish the amount of liquid in the final fill process. This was done by pumping the fully filled heat pipe through a series combination of a needle valve and heated capillary tube. A 61 cm long copper tube with a 0.14 cm outside diameter and 0.063 cm inside diameter was used as the capillary tube. This tube was wound and soldered to a copper cylinder holding a resistance heater and temperature sensor so that the capillary could be temperature controlled at 125°C during use. This insures that the fluid passing through the capillary is in the vapor state to allow precise metering of the methanol. The pressure between the needle valve and capillary was monitored to detect when the heat pipe reached the completely dry state. Typically this pressure was about 110 torr during pump out process and drops rapidly on dry out to indicate when the pump out process is complete.

In addition, the heat pipe substrate was immersed in a temperature controlled bath maintained at 26°C plus or minus 1°C during the pump out process. Typical prototype heat pipes contained 0.80 mg of methanol* when full. This was removed by the metered pumping process in approximately 10 minutes depending on the setting of the needle valve. By pumping for 80% of the full time we could achieve a 20% liquid fill volume with essentially no noncondensable gas in the heat pipe. At this point the soft copper tubing is sealed off by crimping with a pinch off tool.† The precise amount of coolant liquid remaining in the heat pipe was measured using weights determined before and after the fill process.

Material Compatibility between Wall and Coolant

Corrosion Background

Corrosion is the destructive result of chemical reaction between a metal or metal alloy and its environment. It involves two processes: oxidation of the metal and corresponding reduction of another species. Reduction of oxygen or water to produce hydrogen ions are possible examples. Corrosion is often manifest as a thinning of a metal part as the oxidized metal ions enter solution. Additionally, formation of a corrosion product film (metal oxide, sulfide, chloride, or other salt) which remains on the surface can occur. Either situation is potentially a problem for small features such as those in the micro heat pipe wick. Furthermore, corrosion can produce noncondensable gases within the heat pipe that could interfere with the free movement of the coolant vapor.

Corrosion can be accelerated by electrically coupling the metal to another, more noble metal (galvanic coupling). In this case, the active element (anode) in the couple suffers accelerated attack, while the noble metal (cathode) is protected. Galvanic coupling requires

*Methanol 99.9% with < 0.02% water, UN1230 Fisher Scientific, Fair Lawn, NJ.

†MST-1108, Team Co., Brookline, MA.

both ionic and electronic conductivity. Breaking either circuit will eliminate the galvanic effect.

The metals used in the heat pipe are Ni and Kovar (Fe-Ni-Co). As shown in Figure 9, the top and bottom plates, spacer frame, and supports are all constructed of Kovar. The wick features are Ni. In this galvanic couple (Ni to Kovar), the Ni is the cathode and the Kovar acts as the anode. However, the potential difference between the two materials is quite modest and is not expected to accelerate any corrosion process.

A survey of the literature discovered no known compatibility problems with either Kovar or Ni in methanol environments. The corrosion rate for Ni and Ni-base alloys in methanol or methanol/water mixtures was less than 2 mils/year (the lowest category tabulated) for all temperatures tested and for all concentrations. Fe and Fe-base alloys are slightly more susceptible, but all of the corrosion rates reported were less than 20 mils/year, and were less than 2 mils/year when the methanol was kept dry. While even these low tabulated rates are large on the scale of the micro heat pipe features, the small amount of coolant (~170 mg in the present heat pipes) will not sustain such rates.

Potential Test Methods

Three potential techniques were considered to evaluate the corrosion behavior within a micro heat pipe. Two of the techniques, potentiodynamic polarization and electrochemical impedance spectroscopy (EIS), involve instrumenting a sample and measuring the electrochemical response to an applied voltage. The third technique, mass change, requires no electrical contact and does not depend on applying a voltage.

Preliminary attempts at electrochemical tests proved unacceptable. The test requires a minimal level of conductivity of the electrolyte in order to make the measurement. If the methanol is dry (as it is in the current heat pipes), the conductivity is insufficient to allow measurements. Increasing the conductivity through the addition of water or supporting salts influences the corrosion process and is therefore not representative of the actual behavior. Thus, it was concluded that both EIS and DC polarization were inappropriate for this system.

Mass change measurements, on the other hand, place no requirements on electrolyte composition or conductivity. Large area samples of the heat pipe materials were photographed and weighed and placed in dry methanol. The containers were sealed to prevent the introduction of air or water. Visual examination of the samples (after approximately three months of exposure) showed no evidence of attack of either the Ni or the Kovar sheet. This supports the literature data that suggest that an extremely low corrosion rate is expected for both the Kovar and the Ni. Since the exposure testing did not reveal any interaction after three months of exposure, it was decided to allow these tests to continue for a time period beyond the original program termination. At the conclusion of this test, the samples will be weighed and a corrosion rate will be determined.

Destructive Test Methods

The most relevant corrosion evaluation may be the analysis of an actual heat pipe. A cycled heat pipe approximately one year old is currently being evaluated to determine the

composition of the fluid/gas in the interior. Unfortunately, this heat pipe did not become available for destructive analysis until late in the program (since it was being used for thermal analysis and was not of sufficient age), so that the results are not available for this report. The testing is, however, continuing. Following the measurements of liquid and vapor compositions, the device will be opened and metallurgically examined by optical and electron microscopy to determine the location and extent of corrosion experienced during service. It should be noted that prior to initiation of the destructive testing, the thermal characteristics of the device were measured and compared with measurements on the same device taken approximately one year earlier. These comparisons indicated that essentially no degradation of thermal performance had occurred. This observation, coupled with the observation of no apparent interaction between the bulk materials and methanol after three months, implies that the destructive analysis is likely to reveal little or no deleterious interactions within the heat pipe.

Mechanical Design and Wall Deformation

Application of the micro heat pipe substrate to cooling of electronics will involve the use of die bonded to the outer surface of the substrate. Mechanical stresses on the die and adhesive die attach layer are generated by thermal expansion differences between the die and substrate materials. The changing pressure inside the heat pipe can produce additional stresses. In this section, we discuss the mechanical deformation of the heat pipe wall and loads on a silicon die and the die attach layer.

The heat pipe substrate has a hermetically sealed internal cavity containing a wick structure on the internal surfaces. This cavity is partially filled with a liquid coolant. The coolant changes from liquid to vapor to carry heat, which is distributed internally due to capillary action of the wick structure. Electronic die mounted on the exterior of the substrate are cooled effectively by efficient heat transfer from this internal phase change process. The substrate wall material chosen was Kovar, which has a coefficient of thermal expansion (CTE) which more closely matches the CTE of semiconductor die than commonly used substrates. This CTE match is essential for reliable and high thermal conductivity die attachment.

The vapor pressure of the coolant inside the cavity of the heat pipe varies as the temperature changes. Therefore, a fundamental concern was the mechanical design of the cavity wall and support structure. Since microelectronic systems can be directly attached to the low expansion heat pipe substrate, flexure of the substrate due to the internal pressure changes could be detrimental to the reliability of the electronics. It was initially believed that internal support structures that would minimize flexure would also be detrimental to the efficiency of the heat pipe cooling mechanism. The goal of the mechanical design was, therefore, to minimize the heat pipe wall thickness and minimize the number of internal supports without excessive deformation. Such deformation would compromise the attachment of electronics to the substrate. This section reviews the analyses completed to accomplish this task.

Analytic Assessment

In order to establish the initial thickness of the substrate and to determine the necessity for internal supports, a preliminary assessment was completed. For a square flat plate with an applied internal pressure, the maximum flexural displacement, assuming fixed edge boundary conditions, is (from Roark⁷):

$$y = (0.0138pa^4)/(Et^3) \quad (\text{EQ 1})$$

where y = displacement, p = applied pressure, a = length of the side, E = Young's modulus, and t = thickness of plate. For a square flat plate with an applied internal pressure, the maximum flexural displacement, assuming simply supported edge boundary conditions, is:

$$y = (0.0487pa^4(m^2 - 1))/(Et^3m^2) \quad (\text{EQ 2})$$

where $m = 1/\nu$. Assuming $a = 1.5$ inch, $p = 30.0$ psi, $E = 20,000,000.0$ psi, and Poisson's ratio $\nu = 0.17$, the computed displacements are given in Table 5 for assumed substrate thicknesses of 0.020 inch to 0.030 inch.

Table 5: Displacements computed analytically for several substrate thicknesses.

Thickness of Substrate	Computed Displacement Fixed BC	Computed Displacement Simply supported BC
0.020	0.0131	0.0416
0.025	0.0067	0.0213
0.030	0.0039	0.0123

The results in Table 5 suggest that the thickness of the substrate would need to be 0.030 inch or greater to keep the flexure to reasonable values (less than 10% of the thickness). Therefore, some internal supports are required if a wall thickness less than 0.030 inch is desired. Equations 1 and 2 can also be used to estimate the spacing (side dimension = a) of internal supports required for an allowable flexural displacement. The results of this

Table 6: Computed support spacing to maintain displacement below 10% of the substrate thickness.

Thickness of Substrate	Computed Spacing Fixed BC	Computed Spacing Simply supported BC
0.020	0.79	0.59
0.025	0.93	0.70
0.030	1.07	0.8

computation, given in Table 6 suggest that only a few spacers would be needed to keep the flexural displacement to relatively small values.

Finite Element Model

A finite element model of the initial prototype design was developed to more realistically evaluate flexural displacements and stress in the heat pipe substrate. Computations were completed for a bare substrate and for a substrate with an attached silicon die. Figure 18 shows the baseline model (with die) of a 1.9 inch square substrate design with a 1.5 inch square heat pipe cavity and a 0.5 inch square silicon die attached to the center of the outside face of the substrate. The die is 0.025 inch thick with a 0.002 inch die attach layer.

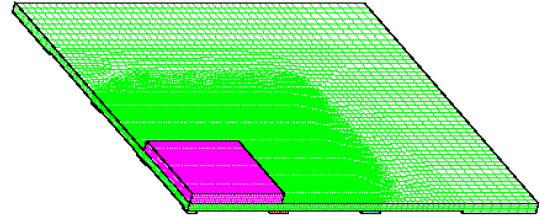


Figure 18. Finite element mesh for baseline structural computations.

Quarter symmetry was taken advantage of in these computations. The model has a series of internal supports which could be selectively activated to study support geometry optimization. All materials were assumed to respond linear elastically. The internal pressure was assumed to be 30 psi, the maximum computed pressure differential that can be developed in the heat pipe. Figure 19 shows the computed displacement contours for

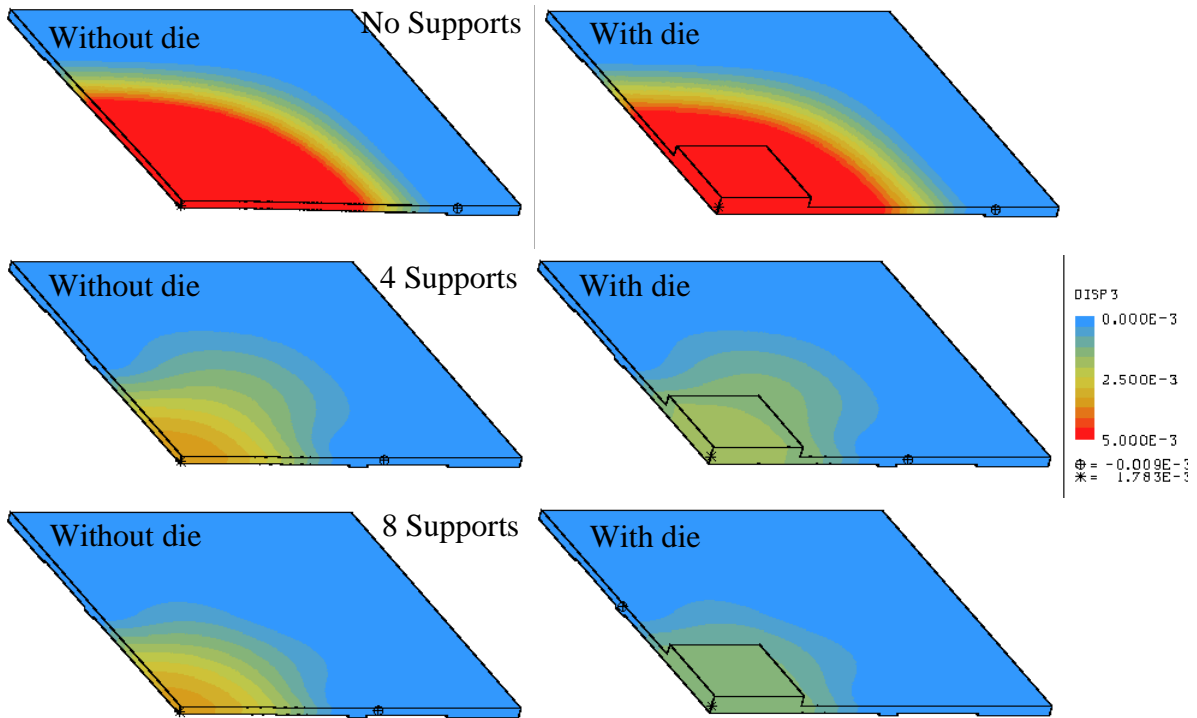


Figure 19. Computed displacement contours for 0, 4, and 8 internal supports for substrate without die and with silicon die. The maximum displacement on the scale is 0.005 inches.

three sets of support conditions. The materials properties used in these computations are given in Table 7. The results of these computations shown in Figure 19 suggest that four internal supports significantly reduce the flexural displacement. Adding four more supports improves flexural displacement only slightly. The computed peak stress in the die attach layer is 5900 psi. This stress value is approximately 20% lower than computed die attach stresses in current production microprocessor packages. Moving the four supports closer to the center of the substrate might help reduce the flexure and stresses but is not required in the current design.

Table 7: Mechanical properties for the materials in the finite element analysis.

Material	Young's Modulus (psi)	Poisson's Ratio
Kovar	20,000,000.0	0.17
Die Attach	1,000,000.0	0.3
Silicon	15,500,000.0	0.2

Summary of the Wall Analysis

Based upon the mechanical analyses, a prototype design was selected using Kovar plates with a wall thickness of 0.020 inch and four internal supports. This design has proven to be adequate in prototype design testing. Not only have the internal spacers proven to be nondetrimental to the heat transfer mechanism; they actually enhance the heat transfer from the lower plate to the upper plate, thus improving heat transfer efficiency.

Thermal Testing

To evaluate the performance of the micro heat pipe substrates, we use a thermal testing system that allows us to measure the temperature distribution on the exterior surfaces of the heat pipe. Temperatures are measured as we apply a known heat input to the surface of the heat pipe, while the temperature at the edge of the heat pipe is constrained to a fixed value. An assembly test die mounted near the center of the heat pipe active surface is used as a heater. A temperature map of the full assembly surface is measured using an infrared imaging system.

Test Die Measurements

The ATC04 assembly test die produced at Sandia is used as the heater for these prototype tests. While this CMOS chip design has a number of stress and temperature diagnostic circuits, we are using only a portion of its features. The chip has four 20 ohm polysilicon heaters that are used in a series-parallel combination to input a selected thermal power for testing. In addition, the die has 25 diodes arrayed across the surface for temperature measurement. In this work, one of those diodes was forward biased with a current of 100 microamps, and the forward biased diode voltage was monitored to determine the temperature on the die. This voltage varies with a temperature coefficient of $-0.554^{\circ}\text{C}/\text{mV}$. The die was mounted on the Kovar heat pipe exterior surface using an epoxy die attach* and cured to a temperature of 150°C for 0.5 hour. The die is nominally 0.59 cm square with

a mounting area of 0.35 cm^2 and is capable of delivering in excess of 20 watts of thermal power to the surface on which it is mounted.

IR measurements

An infrared imaging system* is used to measure detailed temperature profiles on the surface of the operating micro heat pipe prototype. The system includes means for calibration of the detector array, as well as the sample surface emissivity on a pixel-by-pixel basis. A liquid nitrogen cooled InSb detector array has 160 elements in a line and 120 lines of thermal radiance information for a total of 19,200 pixels of measured thermal data in an image. Figure 20 shows the infrared imaging system with its computer for instrument control and display of the test results. The temperature control instrumentation is mounted on the optical stand. The system uses 0.2–1 zoom, 1, 5, and 10 X magnification lenses to cover a range of image sizes. For this work, the 0.2–1X zoom lens was used to frame the area of the heat pipe surface. The detector array charge integration time is selectable to give three calibrated temperature ranges. Depending on the peak temperature, we select the 30–100, 30–200 and 150–300°C ranges. With a high emittance surface these ranges have nominal temperature sensitivities of 0.2, 0.5, and 1°C.

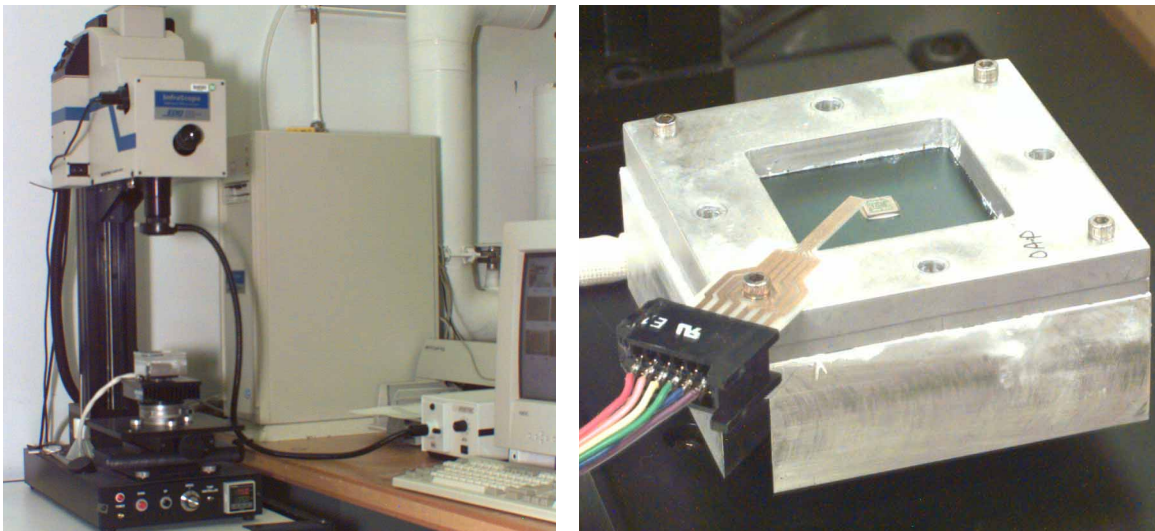


Figure 20. (left) Infrared imaging system and heat pipe mounting fixtures. (right) Detailed view of test fixture seen at the left on the thermal stage below the lens.

The right side of Figure 20 shows a test fixture developed to hold the heat pipe assemblies for thermal measurement. This fixture is attached to the top of the thermoelectric cooler to maintain a controlled temperature selected in the range from 30 to 120°C. The heat pipe substrate can be seen mounted in the middle of an aluminum frame on top of this fixture, where a square area of the heat pipe 3.81 cm (1.5”) on a side is exposed on both sides of the heat pipe. The aluminum frame clamps the outermost 0.51 cm wide area around the

*JM 7000 Die Attach Paste, Johnson Matthey Inc., 10080 Willow Creek Rd., San Diego, CA 92131.

*Edo Barnes Infrascopes, Quantum Focus Inc., 88 Long Hill Cross Roads, Shelton, CN 06484.

edge of the heat pipe surface. This interface between the frame and heat pipe is coated with thermal compound to insure good thermal contact. An ATC04 test die is mounted on one side at the center of the heat pipe exposed area. The wires and interface tab at the lower left of the frame are the electrical connections to the assembly test die. One mil diameter gold wires are bonded between the test die and the interface tab to complete the connections for the heater and temperature sensor. These small-diameter wires reduce conductive heat losses from the die to a negligible level. The aluminum frame on top of the fixture can be inverted, allowing infrared measurements to be done on the back (unheated) face of the operating heat pipe prototype.

The manufacturer specifies a test sequence for calibrating the detector array against a temperature sensor in the thermoelectric controlled temperature stage with a high emittance surface in place of the prototype test fixture. This detector calibration is done before starting the heat pipe tests. Next, the test fixture is mounted in place with the heat pipe prototype.

A temperature map of the heat pipe is acquired with a series of four radiance measurements. First, the system optics are positioned and focused to view the desired region of the test sample. Without disturbing the field of view, we calibrate the emissivity of the sample on a pixel-by-pixel basis. This is done with an automated process of measuring radiance at each location in the image for at least two temperatures. The emissivity is determined with no power applied to the test die. The thermoelectric stage is heated to a specified temperature and after a suitable time for thermal equilibration to a constant temperature across the field of view, a map of the thermal radiance is recorded. Typically 30 to 50 scans of the surface are taken and averaged for each radiance image used. Next the process is repeated at a different temperature, giving a second radiance map. At each pixel these radiance values are subtracted and expressed as a ratio to the difference of the known black body radiance at the two measurement temperatures. These ratios are the pixel-by-pixel emissivity used for temperature calculation.

Next, the thermoelectric stage is set to the desired base temperature for the measurement and a radiance map is taken for the same view undisturbed from the emissivity calibration. Finally, power is applied to the test die and the fourth radiance map is acquired while maintaining the same thermoelectric stage base temperature. The difference of these two radiance values is corrected for the emissivity at each position and added to the known black body radiance at the stage temperature to get the final equivalent powered radiance. This equivalent radiance is used with the original detector calibration to compute the temperatures pixel by pixel. The resulting temperatures are corrected for sample surface emissivity. But also, since the data is taken as a ratio of two measurements, several instrument effects and background thermal effects are cancelled. The full details of this process can be studied in texts devoted to infrared measurement and in the operation manual of the IR system.

Initial Test Results

To illustrate the heat pipe effect in as direct a fashion as possible, two tests were run and compared. The first of these tests used a complete and filled heat pipe. The test used a wick

similar to that shown in Figure 1 and a spacer as shown in Figure 7. This heat pipe was made with two 0.02” thick walls separated by a spacer 0.010” thick. The second test used an equivalent geometry of Kovar walls and spacers, but included no methanol coolant. The comparison of temperatures mapped on the surface of these two substrate configurations is shown in Figure 21.

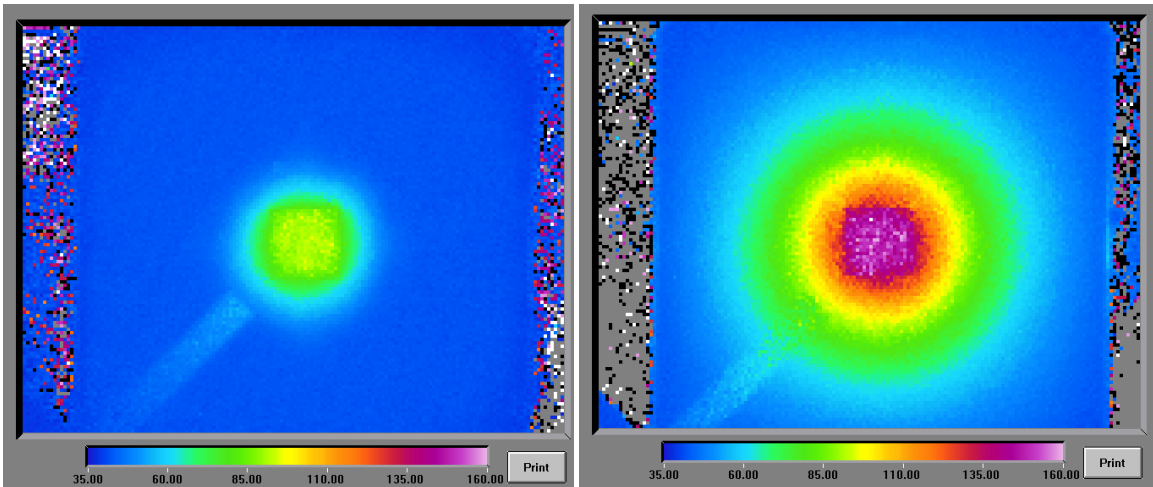


Figure 21. Comparison of a Kovar heat pipe cooled surface (left) to the same geometry of surface without heat pipes (right).

These two measurements both used power input to the test die of 5 watts, corresponding to a flux of approximately 15 W/cm^2 at the die surface and a base temperature on the test fixture of 35°C . Peak temperatures on the die are about 85°C and 160°C . In other words, the temperature rise is 50°C in the heat pipe case, and 125°C in the non-heat pipe case — a factor of 2.5 higher.

This comparison shows the effectiveness of the heat pipe function in cooling a single test die. Thermal data from heat pipe substrate tests such as the one on the left in Figure 21 can also be used to gain additional insight into the details of this heat pipe technology. In the next section, we will discuss some of the modeling of these tests to describe heat pipe thermal performance.

Radial Profile Wick Test

An extensive number of tests with a collection of wick patterns made at various heights were conducted during this work. Analysis of these tests and work to increase the wick height in designs are still under way. Of the collection of tests made to date, among the best performance was found for a radial pattern prototype having relatively tall features. Following is a detailed description of the serial number cd5cd6 prototype test results.

In Figure 22 we show SEM photos of the wick taken at three locations for the wick pattern on the wall used next to the assembly test die: near the substrate center, approximately half way to the edge, and near the edge of the plated area. An increase in the height of the overplated area can be seen for positions nearer the edge of the plated area. This increase is due to the flow of material in the plating bath, an effect that becomes more exaggerated

as the plating speed is increased. In some parts, the overplated area closes off the channels near the edge of the patterned area. This overplating is not a serious problem for the prototypes in these tests, where the heat transfer is concentrated in the center of the heat spreader plate. Some roughness of the surface features can also be seen on this wick. Apparently this roughness does not interfere with the liquid motion, because the prototype shows good heat transfer performance. The height of the wick features near the center of the substrate is 78 μm . This prototype wick height was among the tallest of the features made in tests up to this time. The heat pipe used the second spacer configuration that is shown in Figure 8 and is 0.010" thick. The finished heat pipe was filled with 135 mg of methanol liquid representing 18% of the available internal volume.

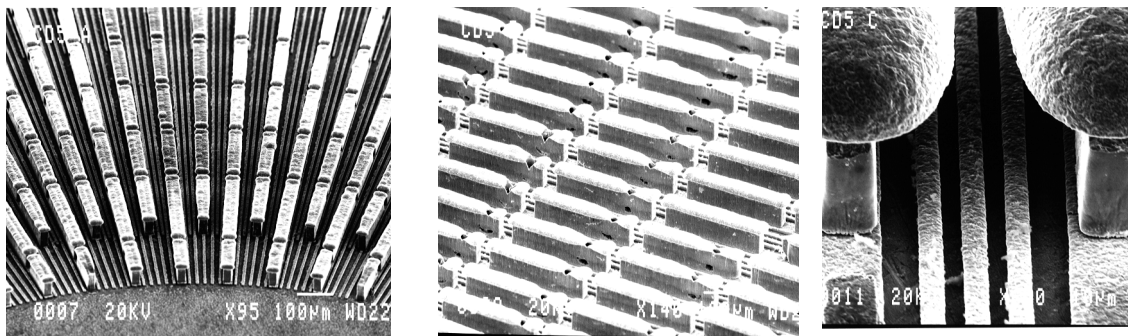
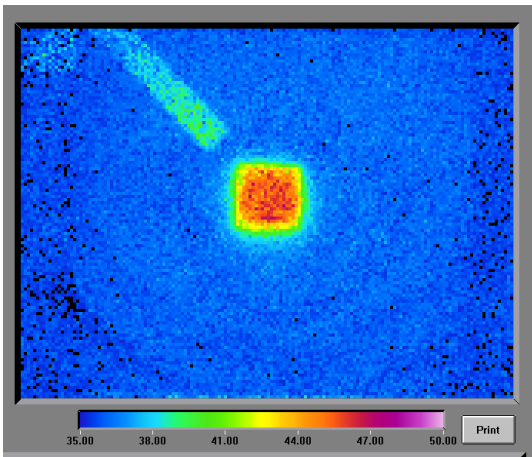


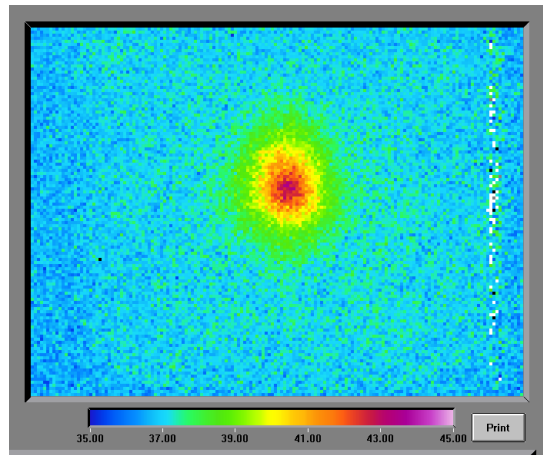
Figure 22. Photo of heated wall wick surface CD5/CD6 prototype at three positions ranging from the center (left) to the outer edge (right). The higher magnification photo at the far right shows the taller overplated cap layer near the edge.

We carried out tests at 2, 5, and 10 watts applied to the test die, with the thermoelectric test stage at 35°C. Measurements were first made on the side of the substrate where the assembly test die is mounted. The mounting frame was then inverted and thermal maps measured at these same power levels on the back side of the substrate opposite to the heat source.

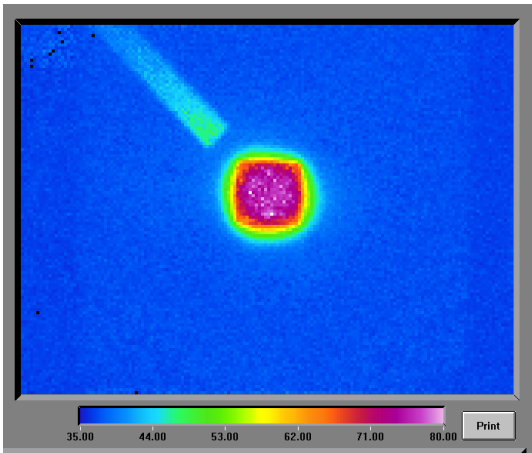
This sequence of temperature measurements is shown in Figure 23. The peak temperature rise at 5 watts power input in this case is 45°C, compared to the rise of 50°C in the test shown in Figure 21. Tests were also done for a base temperature of 55°C on the test stage. Delta T values for the 55°C tests were slightly smaller than for the 35°C base temperature data. This differential may be due to the higher efficiency of the heat pipe at elevated temperatures where the internal pressure and vapor density are greater. However, large differences between the results for the two stage temperatures would indicate the presence of noncondensable gases inside the heat pipe interfering with the performance.



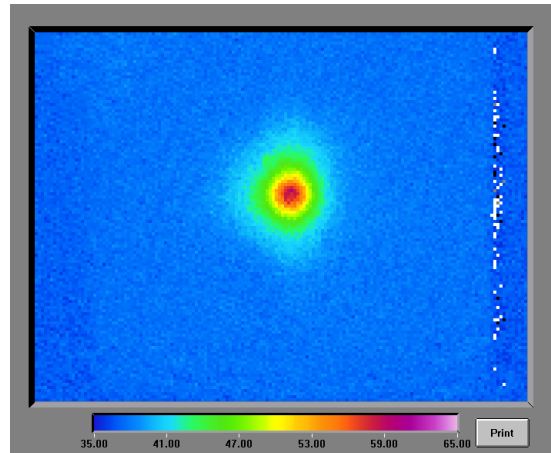
2W 35-50



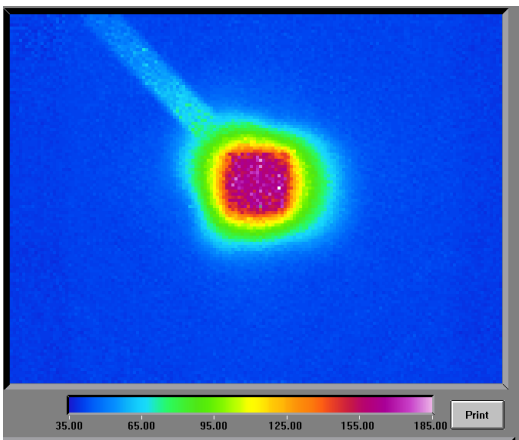
2W 35-45



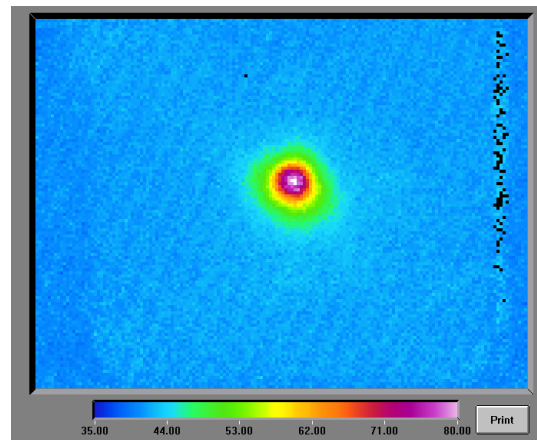
5W 35-80



5W 35-65



10W 35-185



10W 35-80

Figure 23. Front and back temperature maps for 2, 5 and 10 watts power input for the heated side (left) and the back side (right). The base temperature was 35°C for these tests on the CD5CD6 prototype.

Temperature profiles across the front side of the heat pipe were extracted from the image data files. These profiles are plotted in Figure 24 for the full distance in the field of view. Since the die at the center is not coated with a high emissivity surface, the temperature resolution is lower leading to the variations near the peak.

One can see the nonlinear behavior of the heat pipe in these tests. The ΔT values are not in direct proportion to the heater power, but tend to rise faster with increasing power level. Thus the heat pipe becomes less efficient at higher power.

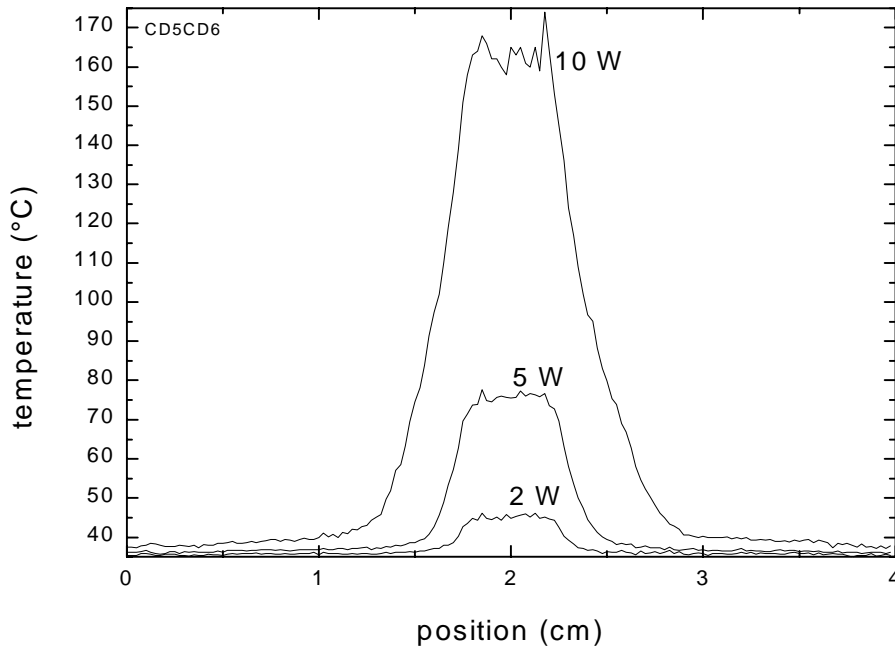


Figure 24. Plots of temperature profiles across CD5CD6 prototype heat pipe for the cases shown in Figure 23.

To help characterize the heat pipe performance we use a simple thermal model. The model is based on experimentally determined heat transfer coefficients rather than first principle descriptions of the fluid drag, pumping pressures, vaporization kinetics, and boiling in the heat pipe. This model allows us to estimate temperatures resulting from variations in power and die placement. A 3D simulation of the test conditions using the known material properties and geometry is used to extract a value for the heat transfer coefficient of the interface layer between the heat pipe wall and fluid. This heat transfer coefficient summarizes the effects of the myriad physical processes in the heat pipe. Thus the coefficient is likely to be a complex function of heat flux for a given geometry.

A value for the heat transfer coefficient is derived from experimental measurements by adjusting the coefficient value until the model matches the experimental temperature profiles. We have found that a single heat transfer coefficient value allows us to estimate temperatures over the range of conditions occurring in these experiments. Also, the cooling effect for multiple die on the heat pipe surface can be determined using this value.

Figure 25 shows the results of this simulation using the geometry of the CD5CD6 heat pipe and a power of 5 watts.

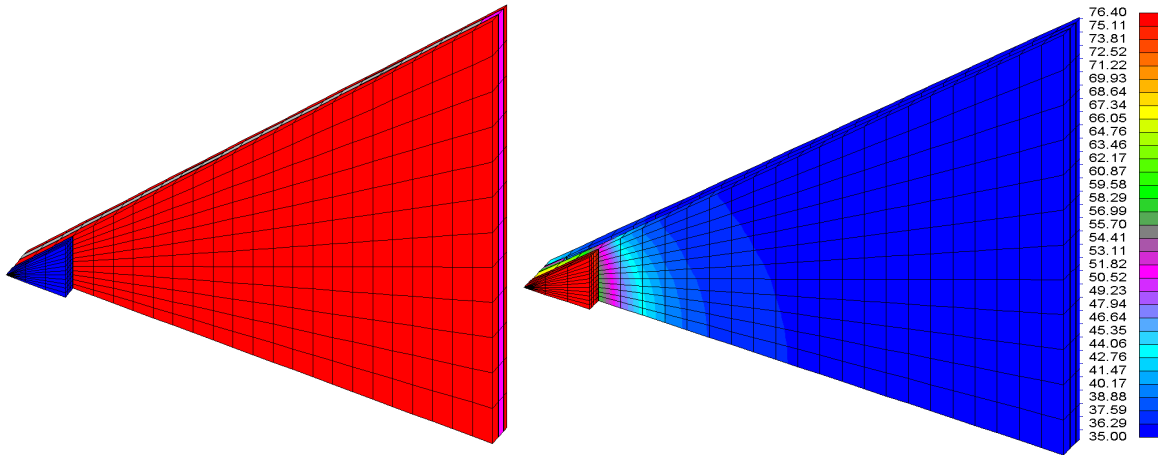


Figure 25. Simulation of a one-eighth section of the CD5CD6 heat pipe geometry, including a die mounted at the center dissipating 5 watts and the edge constrained to a fixed temperature. The colors on the mesh at the left indicate the type of material; the mesh at the right shows a color-coded temperature map of the die and substrate surfaces.

We can directly compare the results of the simulation with the measurements using a profile of surface temperatures. The simulation profile was generated from the center of the die to the edge of the heat pipe for the 5 watt and 35°C base temperature shown in Figure 25. This half profile was mirrored about the heat pipe center and plotted in Figure 26 along with the measured temperature profile from the CD5CD6 test. The calculated profile gives a

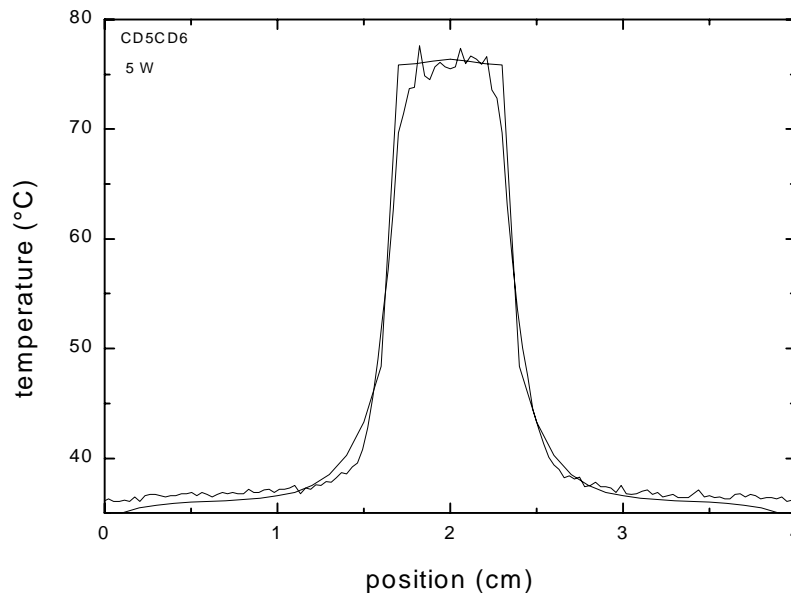


Figure 26. Comparison of temperature profiles from the model and from test results. The model is based on a constant interface heat transfer coefficient.

reasonable comparison to the measured results. This model can be used to estimate temperatures for other power and die placement conditions. Our present simulation uses a constant wall-fluid interface heat transfer coefficient and results in a linear thermal model. Later work will incorporate a temperature dependent heat transfer coefficient to match some of the nonlinear effects seen in the test data.

Discussion

We have described the first steps in the development of a new technology for cooling microelectronics by embedding micro scale heat pipes in a flat plate substrate. Thermal test results from prototype designs that integrate micro heat pipes within substrate walls of Kovar metal show that the addition of micro heat pipes enhances thermal conductivity by a factor of 2.5 over that of Kovar alone. These new substrates are made with relatively low-cost processes and materials.

Future reports will document additional tests we are in the process of performing on variations of the prototype designs. These tests address the radial pattern of wick features, multi-layer designs with narrower wall thicknesses and feature spacing, and two different spacer thicknesses (0.01" and 0.02 "). These design variations have produced only modest variations in performance, with several interesting exceptions: 1) Considerable variation in performance was found among substrates having the same wick geometry. We suspect that this variation may be due to the treatment of the wick surfaces to change the hydrophilic nature of the micro surfaces. 2) The effect of wick height was observed as degraded performance in tests with a short (25 micron high) wick. This result suggests that increasing the aspect ratio (height/width) of features in the wick designs may be a fruitful approach to improving micro heat pipe performance.

Work is needed to address two current limitations of the technology: 1) The prototype designs give useful performance at heat fluxes in the range of $10\text{W}/\text{cm}^2$; further increases in performance will require the development of increased wick heights. Processing developments with advanced etching, lithographic, or LIGA methods are needed in order to attain the high aspect ratios to handle higher heat fluxes. 2) Studies of boiling on the surface of the micromachined structures must be done to better understand the limits of this technology as internal conditions approach wick dryout levels.

With the wick heights presently available, these designs improve the cooling of microelectronic die by factors of 2 to 4. The designs can be useful in moderate heat flux applications where thin substrate and heat spreader geometries are needed to match packaging requirements. They appear particularly useful for 3D packaging where they could be used to carry heat from closely stacked circuit boards. This emerging technology provides designers with a promising new tool for thermal management of increasingly complex microelectronics. By significantly improving the cooling of microelectronic die, micro heat pipe substrates will allow designers to increase their flexibility in packaging, as well as improve the reliability of microelectronics system applications.

References

1. J. Sergent and A. Krum, *Thermal Management Handbook for Electronic Assemblies*, McGraw Hill, New York, 1998.
2. A. Faghri, *Heat Pipe Science and Technology*, Taylor and Francis, Washington D.C., 1995.
3. D. A. Benson, R. T. Mitchell, M. R. Tuck, D. R. Adkins, D. Shen, and D. W. Palmer, "Micro-Machined Heat Pipes in Silicon Substrates," Sandia National Laboratories, SAND97-0100, January 1997.
4. D. A. Benson, R. T. Mitchell, M. R. Tuck, D. W. Palmer, and G. W. Peterson, "Ultrahigh-Capacity Micromachined Heat Spreaders," *Microscale Thermophysical Engineering*, **2**, 1998, 21–30.
5. D. R. Adkins and T. Moss, "Measuring Flow Properties of Wicks for Heat Pipe Solar Receivers," *Solar Engineering*, ed. J. T. Beard, ASME# H00581-90, 1990, 103-108.
6. C. V. Robino, C. R. Hills, and P. F. Hlava, *Low Thermal Expansion Alloys and Composites*, eds. J. J. Stephens and D. R. Frear, TMS, Warrendale, PA, 1994, 123–138.
7. R. J. Roark, *Formulas for Stress and Strain*, McGraw-Hill Book Co., New York, Fourth Edition, 1965.

Appendix A: Parametric Database for the Radial Wick Designs

The first section (“database parameters”) is standard information used to render GDSII files. The “layer numbers” section provides a summary of the overall design. The waferLayer, outerBoundaryLayer, innerBoundaryLayer, and contourLayer are references for visual inspection of the GDSII in a graphical interface environment. The contourLayer and streamLayers were used initially to explore a 2D Laplace geometry, which was superseded by a radial design. The supportLayer and fillLayer are used to provide for vertical supports not part of the wick design but essential in making the heat pipe.

The wick1Layer and wick2Layer correspond to the first generation of radial designs. The wick1ExtensionLayer and wick2ExtensionLayer correspond to additional features added in the second generation radial wick design. The “wick1” and “wick2” sections give geometric details for the two wick layers used in this design.

/*

FILE:HeatPipe2.defaults
CUSTOMER:Dave Benson, 844-1187, dabenso@sandia.gov
CONTACTS:Chris P. Tigges, 844-4453, cptigge@sandia.gov.

NOTES:

(1) User unit assumed to be 1.0(μm)

*/

```
// database parameters
scaleFactor= 1.0;// magnifies structure by
// scaleFactor times
dataBaseUnit= 0.001;// data base unit (grid) in user // units
nVertexes= 100;// number of vertexes used for arc // and circle rendering
outputFilePath= 'HeatPipe2.out';// high level text file
// translation of gds2 file
```

```
// layer numbers
waferLayer= 12;
outerBoundaryLayer= 12;
innerBoundaryLayer= 12;
heatPipeLayer= 1;
contourLayer= 12;
streamLayer= 1;
supportLayer= 3;
```

```
fillLayer= 3;
wick1Layer= 1;
wick1ExtensionLayer= 1;
wick2Layer= 2;
wick2ExtensionLayer= 2;

// wafer (waferLayer)
waferDiameter= 3.0;// (inch)

// outer bounds is a square
outerBoundaryWidth= 1.7;// (inch)

// inner boundary is a circle
innerBoundaryRadius= 200.0; // (μm)

// meshSize for laplace solution
suggestedMeshSize= 500.0;// (μm)
maximumIterations= 20000;// (int)
tolerance= 0.000001;// (ratio)

nContours= 14;// (int)
nStreams= 16;// (int)

// wick1
wick1Width= 20.0;// (μm)
wick1Spacing= 30.0;// (μm)
wick1Mark= 200.0;// (μm)
wick1Space= 25.0;// (μm)
wick1ExtWidthMin= 5.0;// (μm)

// wick2
wick2Width= 4.17;// (μm)
wick2Spacing= 4.16;// (μm), (this is the minimum space)
wick2ExtWidthMin= 1.0;// (μm)
```

Appendix B: Wick Lithography Processes

HEATPIPE 5 Process for dual layer Ni plated features on a Kovar substrate material.

1. Clean in trichloroethylene.
2. Solvent clean wafers with acetone and alcohol.
3. Argon sputter in the Vacutek for 15 min.
4. Coat wafers with 4620. Spin at 2000 rpm for 30 sec.
5. Expose on the MA6 for 13 sec. using the Heat pipe 4 small features mask.
6. Develop in 1:4 for 2:20 sec.
7. Nickel plate small features for 36 amp-min.
8. Strip resist using solvent clean in acetone and alcohol. (DO NOT PLACE WAFERS IN ANY PLASMA CLEAN.)
9. Measure wafer thickness with DekTak wafers at Center, Midpoint and Edge.
10. Coat wafers with 4620. Spin at 900 rpm for 20 sec.
11. Bake at 90°C for 6 min.
12. Cool for 2 min. on cool surface.
13. Coat wafers a second time with 4620. Spin at 900 rpm for 20 sec.
14. Bake at 90°C for 6 min.
15. Cool for 2 min. on cool surface.
16. Expose on the MA6 for 91.2 sec. using the Heat pipe 4 big feature mask.
17. Develop in 421K Developer for 2:15.
18. Dip wafer into Triton X until bubbles are gone.
19. Quickly mount wafer onto Nickel Plater and place into solution before Triton X dries.
20. Nickel plate for 480 amp-min. at a 3 to 7 pulse. The nickel plater should be set up for 6 amps at a zero pulse.
21. Rinse wafer in clean DI water.
22. Solvent clean wafer using acetone and alcohol.
23. Measure plating thickness with DekTak wafers at Center, Midpoint and Edge.
24. Plasma clean for 15 min. using CHF4 program in Lola.

DISTRIBUTION:

- | | |
|---|--|
| 1 David Hamilton, MS 6A-116
U.S. Dept. of Energy Headquarters
Forrestal Building
1000 Independence Ave, S.W.
Washington, DC 20585 | 1 Kevin J. McDunn
Manager, Advanced Products Div.
Motorola
1475 West Shure Drive
Arlington Heights, Illinois 60004 |
| 1 Dr. Yogendra Joshi
University of Maryland
College Park, MD 20742 | 1 Dr. Rainer Dohle
SDL Inc.
80 Rose Orchard Way
San Jose, CA 95134-1365 |
| 1 Prof. Bud Peterson
Dean of Engineering
Texas A&M University
College Station, TX 77843-3126 | 1 Dr. Suraj Rawal
Manager, Advanced Structures,
Materials and Thermal Control
Lockheed Martin Astronautics
P.O. Box 179
Denver, CO 80201-0179 |
| 1 Dr. Robert Palmquist
Via Inc.
11 Bridge Square
Northfield, MN 55057 | 1 Dr. Michael Hmelar
Coherent Semiconductor Group
5100 Patrick Henry Drive
Santa Clara, CA 95054 |
| 1 Mr. Roger A. Baske
CalTrans
10308 Rockbrook Road
Omaha, NE 68124 | 1 Dr. Tom Mix
Merix Corporation
77 Charles street
Needham Heights, MA 02194 |
| 1 Mr. Gene Lussier
Team Serv, LLC
708 N.E. 20th Street
Ft. Lauderdale, FL 33305 | 1 Dr. David Stinton
Oak Ridge National Laboratory
PO Box 2008 MS6063
Oak Ridge TN 37831-6063 |
| 1 Prof. Avi Bar-Cohen
Dept. of Mech. Eng.
Univ. of Minnesota
111 Church St, SE
Minneapolis, MN 55455 | 1 Mr. Stu Weinshenker
Polese Company
10103 Carroll Canyon Rd.
San Diego, CA 92131 |
| 1 Dr. P. W. Runstadler
Applied Thermal Technologies, Inc.
10 Cavendish Court
Lebanon, NH 03766-1442 | 1 Mirjana Vukovic
Nortel Networks
P.O.Box 3511, St. C.,
Ottawa, Ont. K1Y 4H7, Canada |
| 1 Dr. Hongyu Jia
Lucent Technologies,
Mesquite, TX 75149 | |

- 1 Dr. Shri Sridhar
Philips Research
345 Scarborough Rd.
Briarcliff Manor, NY 10510
- 1 Mr. John Pilot
SEMI/SEMATECH
2706 Montopolis Drive
Austin, TX 78741
- 1 Scott D. Garner
Thermacore Inc.
780 Eden Road
Lancaster, PA 17601
- 1 Dr. Marc Zampino
Florida International University
EAS 2441, University Park
Miami FL 33199
- 1 Robin E. Hamilton
Electronic Sensors and Systems Div.
Northrop Grumman Corp., MS 709
P.O. Box 1693
Baltimore, MD 21203
- 2 MS 0899 Technical Library, 4916
- 1 MS 0619 Review and Approval
Desk, 15102 For DOE/OSTI
- 1 MS 0161 Patent & Licensing
Office, 11500
- 1 MS 1079 David Williams, 01700
- 1 MS 0744 D. B. King, 6403
- 1 MS 1425 R.P. Manginell, 1715
- 1 MS 0764 L. Schoeneman, 5825
- 1 MS 0874 D. W. Palmer, 1716
- 1 MS 0874 L. Sloan, 1716
- 1 MS 1082 R.T. Mitchell, 01726
- 1 MS 0603 C. P. Tigges, 01713
- 1 MS 0443 S.N. Burchett, 09117
- 1 MS 0443 H. S. Morgan, 09117
- 1 MS 0603 S. H. Kravitz, 01713
- 5 MS 0367 C. V. Robino, 01833
- 1 MS 0367 B. K. Damkroger, 01833
- 25 MS 1082 D. A. Benson, 1726
- 1 MS 1074 P. V. Dressendorfer,
1726
- 1 MS 0149 C. E. Meyers, 04000
- 1 MS 9018 Central Technical Files,
8940-2